ARTICLE IN PRESS

Journal of Computational Physics xxx (2011) xxx–xxx

Contents lists available at ScienceDirect

Journal of Computational Physics

journal homepage: www.elsevier.com/locate/jcp

The reduced basis method for the electric field integral equation

M. Fares [a], J.S. Hesthaven [b], Y. Maday [c], B. Stamm [d,*]

[a] 2 Avenue Gaspard Coriolis, 31057 Toulouse Cedex 01, France
[b] Division of Applied Mathematics, Brown University, Box F, Providence, RI 02912, USA
[c] Laboratoire Jacques-Louis Lions, Université Pierre et Marie Curie, Boîte courrier 18, 75252 Paris Cedex 05, France
[d] Department of Mathematics, University of California, Berkeley, CA 94720, USA

ARTICLE INFO

Article history:
Received 21 April 2010
Received in revised form 21 January 2011
Accepted 11 March 2011
Available online xxxx

Keywords:
Reduced basis method
Scattering problems
RCS-computations
Boundary Element Method

ABSTRACT

We introduce the reduced basis method (RBM) as an efficient tool for parametrized scattering problems in computational electromagnetics for problems where field solutions are computed using a standard Boundary Element Method (BEM) for the parametrized electric field integral equation (EFIE). This combination enables an algorithmic cooperation which results in a two step procedure. The first step consists of a computationally intense assembling of the reduced basis, that needs to be effected only once. In the second step, we compute output functionals of the solution, such as the Radar Cross Section (RCS), independently of the dimension of the discretization space, for many different parameter values in a many-query context at very little cost. Parameters include the wavenumber, the angle of the incident plane wave and its polarization.

1. Introduction

Many applications related to computational optimization, control and design, require the ability to rapidly, perhaps even in real time, and accurately predict some output under the variation of a set of parameters. A similar need can be found in the development of large simulation based databases or the development of efficient way to quantify uncertainty and its impact.

In such cases, the solution is often implicitly related to a set of parameters $\underline{\boldsymbol{\mu}}$, which denotes the input. In practice the parameters can be related to the description of sources, materials, geometries, uncertainties and so on. In such cases we have an implicit relationship between the input and the output through the partial differential equation.

In this work we shall pursue the development of efficient and accurate computational methods for problems of electromagnetics. In particular we shall discuss the methods based on the electric field integral equation (EFIE) [18], given on abstract form as

$$a(\underline{\mathbf{J}}(\underline{\boldsymbol{\mu}}),\underline{\mathbf{J}}_t;\underline{\boldsymbol{\mu}}) = f(\underline{\mathbf{J}}_t;\underline{\boldsymbol{\mu}}), \quad \forall \underline{\mathbf{J}}_t \in \boldsymbol{V},$$

where the parameter space is denoted by $\mathcal{D}$, $\boldsymbol{V}$ is some appropriate functional space and $a(\cdot,\cdot;\underline{\boldsymbol{\mu}})$, $f(\cdot;\underline{\boldsymbol{\mu}})$ a sesquilinear resp. linear form for any parameter value $\underline{\boldsymbol{\mu}} \in \mathcal{D}$.

Our primary goal is to develop a systematic approach to obtain an accurate and reliable approximation of the output of interest at very low computational cost for applications where many queries, i.e., solutions, are needed. We shall explore the use of a reduced basis method by recognizing, and implicitly assuming, that the parameter dependent solution is not simply

---

[*] Corresponding author.

E-mail addresses: fares@cerfacs.fr (M. Fares), Jan_Hesthaven@Brown.edu (J.S. Hesthaven), maday@ann.jussieu.fr (Y. Maday), stamm@math.berkeley.edu (B. Stamm).

0021-9991/$ - see front matter © 2011 Elsevier Inc. All rights reserved.
doi:10.1016/j.jcp.2011.03.023

Please cite this article in press as: M. Fares et al., The reduced basis method for the electric field integral equation, J. Comput. Phys. (2011), doi:10.1016/j.jcp.2011.03.023

an arbitrary member of the infinite-dimensional space associated with the partial differential equation, but rather that it evolves on a lower-dimensional manifold induced by the parametric dependence.

On a discrete level, this assumption can computationally be tested for particular cases. To do so, consider the underlying abstract discrete problem: for any given parameter value $\underline{\boldsymbol{\mu}} \in \mathcal{D}$, find $\underline{\mathbf{J}}_h \in \boldsymbol{V}_h$ such that

$$a(\underline{\mathbf{J}}_h(\underline{\boldsymbol{\mu}}), \underline{\mathbf{J}}_t; \underline{\boldsymbol{\mu}}) = f(\underline{\mathbf{J}}_t; \underline{\boldsymbol{\mu}}), \quad \forall \underline{\mathbf{J}}_t \in \boldsymbol{V}_h, \tag{1}$$

where $\boldsymbol{V}_h$ is an appropriate discrete subspace of $\boldsymbol{V}$. Then, compute a singular value decomposition (SVD) of the matrix consisting of the column-wise representation of the numerical approximations $\underline{\mathbf{J}}_h(\underline{\boldsymbol{\mu}})$ for different values $\underline{\boldsymbol{\mu}}$ of a fine point discretization Ξ of the parameter space $\mathcal{D}$.

In order to obtain the numerical solution, any reasonable standard solver can be used. In the framework of this work, we have focused on the Boundary Element Method using the lowest order Raviart–Thomas elements also called Rao–Wilton–Glisson basis [32]. However, the setting is not restricted to the particular choice. These solutions are what we define as the truth solutions and which we seek to approximate.

The left eigenvectors of the SVD corresponding to the N most significant singular values build an ideal reduced basis. More precisely the numerical solution for any particular parameter value $\underline{\boldsymbol{\mu}} \in \Xi$ can be approximated by a linear combination of the left eigenvectors up to a precision of the $(N+1)$-th singular value (in the l^2-norm). Therefore any numerical solution can be represented, up to a certain precision, using the low dimensional subspace spanned by the left eigenvectors of the SVD.

Fig. 1(a) plots the singular values of the matrix consisting of column-wise boundary element solutions for different wave numbers and incident wave directions of an incident plane wave being diffracted on a scatterer illustrated in Fig. 3. In particular, the incident wave direction is expressed in spherical coordinates and we consider the case of $(k, \theta) \in [0, 25] \times [0, \pi]$ and $\phi = 0$ fixed. We observe exponential convergence for the first singular values and note that an error in the current of 10^{-7} can be achieved with 200 basis functions.

In Fig. 1(b), different types of SVD-profiles are plotted. Case 1 is the repetition of the real case of the figure (a) and case 2 is a perfect exponential decrease of the singular values. Case 3 illustrates a (hypothetical) case of a problem where the discrete solution space can not be represented by a low dimensional subspace and no exponential convergence for the first singular values is observed.

In the framework of parametrized scattering problems the exponential decay of the singular values is an essential assumption and reasonable for the types of applications considered here. In what follows, we therefore make the following assumption:

Assumption 1.1 (*Existence of a low dimensional reduced basis*). The subspace $\mathcal{M}_h := \{\underline{\mathbf{J}}_h(\underline{\boldsymbol{\mu}}) | \forall \underline{\boldsymbol{\mu}} \in \mathcal{D}\}$,where $\underline{\mathbf{J}}_h(\underline{\mu})$ is the numerical solution of the EFIE for $\underline{\mu}$ defined by (1), is of low dimensionality, i.e.

$$\mathcal{M}_h \overset{Tol}{=} \mathrm{span}\{\underline{\zeta}_i | i = 1, \ldots, N\}$$

up to a certain given tolerance *Tol* for some properly chosen $\{\underline{\zeta}_i\}_{i=1}^N$ (left eigenvectors of the SVD) and moderate $N \ll \mathcal{N} = \dim(\textit{Discretization space})$. More precisely, we assume that the relation between the achieved tolerance *Tol* with respect to the number of elements N of the “ideal” reduced basis is exponentially decreasing.

Under this assumption we can expect that as $\underline{\boldsymbol{\mu}}$ varies, the set of all solutions can be well approximated by a finite and low dimensional vector space.

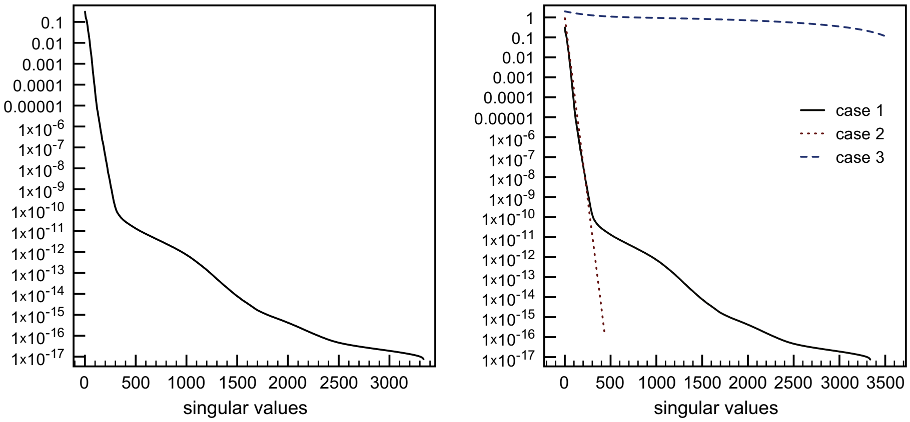

Fig. 1. Singular value decomposition of the matrix consisting of column-wise boundary element solutions for different parameters values of a real case (a). Different types of SVD-profiles (b).

Please cite this article in press as: M. Fares et al., The reduced basis method for the electric field integral equation, J. Comput. Phys. (2011), doi:10.1016/j.jcp.2011.03.023

The basic of the reduced basis method was first introduced in the 1970's for nonlinear structural analysis [1,28] and it was subsequently abstracted, analyzed [4,34] and generalized to other type of parametrized partial differential equations [17,29]. Most of these earlier works focus on arguments that are local in the parameter space. Expansions to a low dimensional manifold are typically defined around a particular point of interest and the associated a priori analysis relies on asymptotic arguments on sufficiently small neighborhoods [14,30]. In such cases, the computational improvements are quite modest. In [2,21] a global approximation space was built by using solutions of the governing PDE at globally sampled points in the parameter space, resulting in a much more efficient method. However, no a priori theory or a posteriori error estimators were developed in this early work.

In recent years, a number of novel ideas and essentially new features have been presented [3,16,22,24,31,35,37–39]. In particular, global approximation spaces are used and uniform exponential convergence of the reduced basis approximation has been numerically observed and confirmed in [25] where the first theoretical a priori convergence result for a one dimensional parametric space problem is presented. The development of rigorous a posteriori error estimators has also been presented, thereby transforming the reduced basis methods from an experimental technique to a computational method with a true predictive value.

Furthermore, in cases where the problem satisfies an affine assumption; that is, the operators and the data can be written as a linear combination of functions with separable dependence of the parameter and the spatial variation of the data, an off–line/on–line computational strategy can be formulated. The off–line part of the algorithm, consisting of the generation of the reduced basis space, is $\underline{\mu}$-independent and can be done in preprocessing. The computational cost of the on–line part depends solely on the dimension of the reduced basis space and the parametric complexity of the problem, while the dependence on the complexity of the truth approximation has been removed, resulting in a highly efficient approach.

While there is substantial past work on the development of reduced basis methods for both coercive and non-coercive problems [27,31,36,9], the majority of the past work has been done based on partial differential equations. However, many problems of industrial and applied character are more efficiently solved using integral equations, i.e., computational techniques based on a direct discretization of the electric/magnetic/combined fields integral equations [18] continues be the preferred and most efficient approach for large scale electromagnetic computations.

Apart from numerous central computational and mathematical differences introduced by the focus on integral equations, an essential difference that emerges is the lack of affine operators, required to ensure an efficient online/offline separation. Unless this is addressed in detail, as we do here, the computational cost of the overall algorithm is not achieved. In this work we continue the work in [3] and present a significant extension of this work to ensure accuracy and efficiency by an *hp*-like empirical interpolation method.

In Section 2 we introduce the underlying physical problem and derive its representation as an integral equation which depends on the parameter values. Section 3 explains how the problem can be solved using the standard Boundary Element Method (BEM) for a fixed parameter value. The reduced Basis method in combination with the BEM in an algorithmic cooperation (rather than a competition) is then applied to solve the general parametrized problem in Section 4. A key-tool for this type of integral equation, due to the non-affine nature of the kernel function, is the Empirical Interpolation Method (EIM) introduced in Section 5. It is further developed to shift the workload from the Online part of the RBM to Offline part resulting in the Elementwise Empirical Interpolation Method (EEIM). Finally, in Section 6 we present some numerical examples of the RBM and we draw our conclusions in Section 7.

2. Parametrized electric field integral equation (μEFIE)

The underlying physical problem is the following: An incident plane wave $\underline{\mathbf{E}}^{inc}$ is scattered at the surface of a perfect conductor, see Fig. 2, obeying Maxwell's equations and the Silver–Müller radiation condition at infinity. The resulting scattered

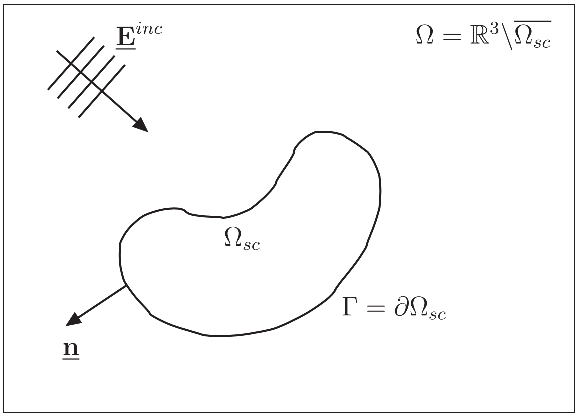

Fig. 2. Illustration of the problem setting.

electric field is denoted by $\underline{\mathbf{E}}^{sc}$. The perfect conductor can either have a volume or simply consist of a surface and is denoted by Ω_{sc}. Its complement is denoted by $\Omega = \mathbb{R}^3 \setminus \overline{\Omega_{sc}}$ and its surface by Γ, with the outer unit normal $\underline{\mathbf{n}}$. Whenever the scatterer consists only of a surface, no outer resp. inner normal can be defined and we use an arbitrary but fixed convention for $\underline{\mathbf{n}}$. The magnetic permeability μ and electric permittivity ε are assumed to be homogeneous in Ω.

Denote by $\underline{\mathbf{E}}$ the total electric field and by $\underline{\mathbf{H}}$ the magnetic field. Under the assumption of a harmonic time dependence, the electric and magnetic complex fields $\underline{\mathbf{E}}, \underline{\mathbf{H}} \in \boldsymbol{H}_{\text{curl}}(\Omega)$ satisfy

$$i\omega\mu\underline{\mathbf{H}} - \text{curl}\underline{\mathbf{E}} = 0 \quad \text{in } \Omega, \tag{2}$$

$$i\omega\varepsilon\underline{\mathbf{E}} + \text{curl}\underline{\mathbf{H}} = 0 \quad \text{in } \Omega, \tag{3}$$

with $\omega > 0$ being the angular frequency. It is convenient to introduce the wavenumber k and the impedance Z

$$k = \omega\sqrt{\mu\varepsilon},$$

$$Z = \sqrt{\mu/\varepsilon}.$$

Then, $i\omega\mu = ikZ$, $ik\varepsilon = ik/Z$ and substituting (2) into (3) yields

$$\text{curl curl } \underline{\mathbf{E}} - k^2\underline{\mathbf{E}} = 0 \quad \text{in } \Omega. \tag{4}$$

In addition we assume the Silver–Müller radiation condition at infinity

$$\left|\text{curl}\underline{\mathbf{E}}^{sc}(\underline{\mathbf{x}}) \times \frac{\underline{\mathbf{x}}}{|\underline{\mathbf{x}}|} - ik\underline{\mathbf{E}}^{sc}(\underline{\mathbf{x}})\right| = \mathcal{O}\left(\frac{1}{|\underline{\mathbf{x}}|}\right) \quad \text{as } |\underline{\mathbf{x}}| \to \infty \tag{5}$$

and the boundary condition

$$\underline{\gamma_t}\underline{\mathbf{E}} = \underline{\mathbf{0}} \quad \text{on } \Gamma$$

since the body Ω_{sc} is assumed to be a perfectly conducting scatterer. Here, $\underline{\gamma_t}$ denotes the tangential trace operator on the surface Γ defined by $\underline{\gamma_t}\underline{\mathbf{v}} = \underline{\mathbf{n}} \times (\underline{\mathbf{v}} \times \underline{\mathbf{n}})$ for sufficiently smooth $\underline{\mathbf{v}}$ and surface Γ. As our interest is the scattering of an incident plane wave by the surface Γ of the perfect conductor Ω_{sc} we write

$$\underline{\mathbf{E}}(\underline{\mathbf{x}}) = \underline{\mathbf{E}}^{inc}(\underline{\mathbf{x}}) + \underline{\mathbf{E}}^{sc}(\underline{\mathbf{x}}) \quad \text{with } \underline{\mathbf{E}}^{inc}(\underline{\mathbf{x}}) = \underline{\mathbf{p}}e^{ik\hat{\underline{\mathbf{k}}}\cdot\underline{\mathbf{x}}}, \tag{6}$$

where the unit vector $\hat{\underline{\mathbf{k}}}$ denotes the wave direction and $\underline{\mathbf{p}}$ the polarization (lying in the plane perpendicular to $\hat{\underline{\mathbf{k}}}$). Note that $\underline{\mathbf{E}}^{inc}$ is assumed to satisfy (4). Thus the unknown is no longer the total field $\underline{\mathbf{E}}$ but the scattered field $\underline{\mathbf{E}}^{sc}$ with the boundary condition

$$\underline{\gamma_t}\underline{\mathbf{E}}^{sc} = -\underline{\gamma_t}\underline{\mathbf{E}}^{inc} \quad \text{on } \Gamma.$$

Next, we introduce a new unknown tangential vector field $\underline{\mathbf{J}}$, the electric current on the surface Γ (being $\underline{\mathbf{J}} = \underline{\mathbf{n}} \times \underline{\mathbf{H}}|_\Gamma$ on the surface for closed surfaces Γ). Denote by $\boldsymbol{H}_{\text{curl}}(\Omega)$ the natural solution space of Maxwell's equations in Ω and define $\boldsymbol{H}_{\text{div}}^{-\frac{1}{2}}(\Gamma)$ as the trace space of $\underline{\mathbf{n}} \times \boldsymbol{H}_{\text{curl}}(\Omega)$ on the surface, see [5–8,10] for different types of surfaces. The electric and magnetic field $\underline{\mathbf{E}}$, $\underline{\mathbf{H}}$ can be represented in Ω depending solely on the electric and magnetic current on the body, a result known as the Stratton–Chu representation formula. In the case of a perfect conductor, it simplifies to

$$\underline{\mathbf{E}}(\underline{\mathbf{x}}) = \underline{\mathbf{E}}^{inc}(\underline{\mathbf{x}}) + ikZ\underline{\mathbf{T}_k}\underline{\mathbf{J}}(\underline{\mathbf{x}}), \tag{7}$$

where the (linear) potential $\underline{\mathbf{T}}_k$ is defined as

$$\underline{\mathbf{T}_k}\underline{\mathbf{J}}(\underline{\mathbf{x}}) = \int_\Gamma \left[G(r;k)\underline{\mathbf{J}}(\underline{\mathbf{y}}) + \frac{1}{k^2}\nabla_{\Gamma,x}G(r;k)\text{div}_{\Gamma,y}\underline{\mathbf{J}}(\underline{\mathbf{y}})\right]d\underline{\mathbf{y}}$$

in Ω with $r = |\underline{\mathbf{x}} - \underline{\mathbf{y}}|$ and where $G(\cdot;k)$ is the fundamental solution of the Helmholtz operator $\Delta + k^2$ given as

$$G(r,k) = \frac{e^{ikr}}{4\pi r}.$$

Applying the tangential trace to (7) and invoking the boundary condition for $\underline{\mathbf{E}}$ yields the electric field integral equation (EFIE):

$$ikZ\underline{\mathbf{S}_k}\underline{\mathbf{J}}(\underline{\mathbf{x}}) = -\underline{\gamma_t}\underline{\mathbf{E}}^{inc}(\underline{\mathbf{x}}), \tag{8}$$

where the boundary potential $\underline{\mathbf{S}}_k$ is defined as

$$\underline{\mathbf{S}_k} = \underline{\gamma_t} \circ \underline{\mathbf{T}_k}.$$

Let $\underline{\mathbf{J}_t} \in \boldsymbol{H}_{\text{div}}^{-\frac{1}{2}}(\Gamma)$ be a test function, then the weak form of the EFIE reads: find $\underline{\mathbf{J}} \in \boldsymbol{H}_{\text{div}}^{-\frac{1}{2}}(\Gamma)$ such that

$$ikZ\int_\Gamma \underline{\mathbf{S}_k}\underline{\mathbf{J}}(\underline{\mathbf{x}}) \cdot \overline{\underline{\mathbf{J}_t}(\underline{\mathbf{x}})}\underline{\mathbf{dx}} = -\int_\Gamma \underline{\gamma_t}\underline{\mathbf{E}}^{inc}(\underline{\mathbf{x}}) \cdot \overline{\underline{\mathbf{J}_t}(\underline{\mathbf{x}})}\underline{\mathbf{dx}}$$

Please cite this article in press as: M. Fares et al., The reduced basis method for the electric field integral equation, J. Comput. Phys. (2011), doi:10.1016/j.jcp.2011.03.023

for all test functions $\underline{\mathbf{J}}_t \in \boldsymbol{H}_{\mathrm{div}}^{-\frac{1}{2}}(\Gamma)$, and where $\overline{\underline{\mathbf{J}}_t(\underline{\mathbf{x}})}$ denotes the complex conjugate of $\underline{\mathbf{J}}_t(\underline{\mathbf{x}})$. Applying integration by parts then yields: find $\underline{\mathbf{J}} \in \boldsymbol{H}_{\mathrm{div}}^{-\frac{1}{2}}(\Gamma)$ such that

$$a(\underline{\mathbf{J}}, \underline{\mathbf{J}}_t) = f(\underline{\mathbf{J}}_t) \quad \forall \underline{\mathbf{J}}_t \in \boldsymbol{H}_{\mathrm{div}}^{-\frac{1}{2}}(\Gamma),$$

with, using the notation $r = |\underline{\mathbf{x}} - \underline{\mathbf{y}}|$,

$$a(\underline{\mathbf{J}}, \underline{\mathbf{J}}_t) = ikZ \int_\Gamma \int_\Gamma G(r;k) \left[\underline{\mathbf{J}}(\underline{\mathbf{x}}) \cdot \overline{\underline{\mathbf{J}}_t(\underline{\mathbf{y}})} - \frac{1}{k^2} \mathrm{div}_{\Gamma,\underline{\mathbf{x}}} \underline{\mathbf{J}}(\underline{\mathbf{x}}) \mathrm{div}_{\Gamma,\underline{\mathbf{y}}} \overline{\underline{\mathbf{J}}_t(\underline{\mathbf{y}})} \right] \underline{\mathbf{dx}}\,\underline{\mathbf{dy}},$$

$$f(\underline{\mathbf{J}}_t) = -\int_\Gamma \gamma_t \underline{\mathbf{E}}^{inc}(\underline{\mathbf{y}}) \cdot \overline{\underline{\mathbf{J}}_t(\underline{\mathbf{y}})} \underline{\mathbf{dy}}.$$

Let us now introduce the parametrized EFIE. To do so, let the unit wave direction $\underline{\hat{\mathbf{k}}}$ be parametrized in spherical coordinates (θ, φ), i.e.

$$\underline{\hat{\mathbf{k}}} = -\begin{pmatrix} \cos(\varphi)\sin(\theta) \\ \sin(\varphi)\sin(\theta) \\ \cos(\theta) \end{pmatrix}, \quad \theta \in [0, \pi], \ \varphi \in [0, 2\pi).$$

Further, the plane perpendicular to $\underline{\hat{\mathbf{k}}}$ can be parametrized by the two following basis vectors

$$\underline{\mathbf{e}}_\theta = \begin{pmatrix} \cos(\varphi) cos(\theta) \\ \sin(\varphi)\cos(\theta) \\ -\sin(\theta) \end{pmatrix} \quad \text{and } \underline{\mathbf{e}}_\varphi = \begin{pmatrix} -\sin(\varphi) \\ -\cos(\varphi) \\ 0 \end{pmatrix}.$$

The polarization in (6) is given by $p_\theta, p_\varphi \in \mathbb{C}$ such that

$$\underline{\mathbf{p}} = p_\theta \underline{\mathbf{e}}_\theta + p_\varphi \underline{\mathbf{e}}_\varphi.$$

The EFIE problem is parametrized by a 7-tuple $\underline{\boldsymbol{\mu}} \in \mathbb{R}^7$, $\underline{\boldsymbol{\mu}} = (k, \theta, \varphi, p_\theta^r, p_\theta^i, p_\varphi^r, p_\varphi^i)$, where:

k: is the wave number,
θ: is the first spherical coordinate of the wave direction $\underline{\hat{\mathbf{k}}}$,
φ: is the second spherical coordinate of the wave direction $\underline{\hat{\mathbf{k}}}$,
p_θ^r: is the real part of p_θ,
p_θ^i: is the imaginary part of p_θ,
p_φ^r: is the real part of p_φ,
p_φ^i: is the imaginary part of p_φ.

For notational convenience we use the abbreviation $\underline{\boldsymbol{\mu}} = (k, \underline{\hat{\mathbf{k}}}, \underline{\mathbf{p}})$ and generally assume that the parameter values lie in the parameter domain $\mathcal{D} \subset \mathbb{R}^p$, with $1 \leqslant p \leqslant 7$ active parameters.

It is well-known [10,19] that the EFIE is not well-posed for scatterers with volume and where k is a resonant wavenumber, i.e. if the interior Maxwell problem on Ω_{sc} for k does not have a unique solution for homogeneous boundary conditions. Let us denote by K_0 the spectrum of resonant wave numbers, i.e. $K_0 = \{k_1, k_2, \ldots\}$, in the case of dealing with a scatterer with a volume. We assume that $K_0 \cap \mathcal{D} = \emptyset$.

The *parametrized* electric field integral equation reads: For any fixed parameter value $\underline{\boldsymbol{\mu}} \in \mathcal{D}$, find $\underline{\mathbf{J}}(\underline{\boldsymbol{\mu}}) \in \boldsymbol{H}_{\mathrm{div}}^{-\frac{1}{2}}(\Gamma)$ such that

$$a(\underline{\mathbf{J}}(\underline{\boldsymbol{\mu}}), \underline{\mathbf{J}}_t; \underline{\boldsymbol{\mu}}) = f(\underline{\mathbf{J}}_t; \underline{\boldsymbol{\mu}}) \quad \forall \underline{\mathbf{J}}_t \in \boldsymbol{H}_{\mathrm{div}}^{-\frac{1}{2}}(\Gamma),$$

with

$$a(\underline{\mathbf{J}}, \underline{\mathbf{J}}_t; \underline{\boldsymbol{\mu}}) = ikZ \int_\Gamma \int_\Gamma G(r;k) \left[\underline{\mathbf{J}}(\underline{\mathbf{x}}) \cdot \overline{\underline{\mathbf{J}}_t(\underline{\mathbf{y}})} - \frac{1}{k^2} \mathrm{div}_{\Gamma,\underline{\mathbf{x}}} \underline{\mathbf{J}}(\underline{\mathbf{x}}) \mathrm{div}_{\Gamma,\underline{\mathbf{y}}} \overline{\underline{\mathbf{J}}_t(\underline{\mathbf{y}})} \right] \underline{\mathbf{dx}}\,\underline{\mathbf{dy}},$$

$$f(\underline{\mathbf{J}}_t; \underline{\boldsymbol{\mu}}) = -\int_\Gamma \gamma_t \underline{\mathbf{E}}^{inc}(\underline{\mathbf{y}}; \underline{\boldsymbol{\mu}}) \cdot \overline{\underline{\mathbf{J}}_t(\underline{\mathbf{y}})} \underline{\mathbf{dy}}.$$

Note that the sesquilinear form a is only dependent on the parameter k, and not on the other parameters. Therefore, we also use $a(\underline{\mathbf{J}}, \underline{\mathbf{J}}_t; k)$ as notation when the sole dependence on k shall be highlighted.

2.1. Output functional: Radar Cross Section (RCS)

The output of interest in parametrized scattering problems is the Radar Cross Section (RCS) as an indication of the far field associated with a scatterer. The RCS is a functional of the electric current $\underline{\mathbf{J}}$ on the surface and is defined by

Please cite this article in press as: M. Fares et al., The reduced basis method for the electric field integral equation, J. Comput. Phys. (2011), doi:10.1016/j.jcp.2011.03.023

$$\mathrm{RCS}(\underline{\mathbf{J}};\hat{\underline{\mathbf{d}}},k) := 10\log_{10}\left(4\pi\frac{|\underline{\mathbf{s}}_\infty(\underline{\mathbf{J}};\hat{\underline{\mathbf{d}}},k)|^2}{|\underline{\mathbf{E}}^{inc}(\underline{\boldsymbol{\mu}})|^2}\right),$$

where $\underline{\mathbf{s}}_\infty$ is a linear functional of the electric current $\underline{\mathbf{J}}$ given by

$$\underline{\mathbf{s}}_\infty(\underline{\mathbf{J}};\hat{\underline{\mathbf{d}}},k) := \frac{ikZ}{4\pi}\int_\Gamma \hat{\underline{\mathbf{d}}}\times(\underline{\mathbf{J}}\times\hat{\underline{\mathbf{d}}})e^{ik\underline{\mathbf{x}}\cdot\hat{\underline{\mathbf{d}}}}\underline{\mathbf{dx}}$$

for some given directional unit vector $\hat{\underline{\mathbf{d}}}$. The RCS signal describes the energy of the total electric field $\underline{\mathbf{E}}$ at infinity towards the direction

$$\hat{\underline{\mathbf{d}}} = \begin{pmatrix}\cos(\varphi_{\mathrm{rcs}})\sin(\theta_{\mathrm{rcs}})\\ \sin(\varphi_{\mathrm{rcs}})\sin(\theta_{\mathrm{rcs}})\\ \cos(\theta_{\mathrm{rcs}})\end{pmatrix}, \quad \theta_{\mathrm{rcs}}\in[0,\pi],\ \varphi_{\mathrm{rcs}}\in[0,2\pi).$$

3. BEM for the EFIE with fixed parameter

For any fixed parameter value, the EFIE can subsequently be discretized using a Galerkin approach. Replacing the functional space $\boldsymbol{H}_{\mathrm{div}}^{-\frac{1}{2}}(\Gamma)$ by some conforming finite dimensional subspace yields the Boundary Element Method (BEM), also called Method of Moment (MoM). A common choice as discretization space is the lowest order complex Raviart–Thomas space $\boldsymbol{RT}_0$, also called the Rao–Wilton–Glisson elements in the electromagnetic community.

Let $\mathcal{T}_h$ be a family of shape-regular triangulations decomposing Γ into flat triangles. For a fixed triangulation let h_T denote the mesh size of any element $T\in\mathcal{T}_h$ and let $\mathtt{h}$ be the elementwise constant function such that $\mathtt{h}|_T = h_T$.

By $\boldsymbol{RT}_0(T)$ we denote the local Raviart–Thomas space on Γ of complex-valued functions on $T\in\mathcal{T}_h$ defined by (cf. [13,33])

$$\boldsymbol{RT}_0(T) := \left\{\underline{\mathbf{v}}_h(\underline{\mathbf{x}}) = \underline{\alpha} + \beta\underline{\mathbf{x}} | \underline{\alpha}\in\mathbb{C}^2,\ \beta\in\mathbb{C},\ \underline{\mathbf{x}}\in T\right\}.$$

On a global level, the Raviart–Thomas space is defined by

$$\boldsymbol{RT}_0 := \left\{\underline{\mathbf{v}}_h \in \boldsymbol{H}^0_{\mathrm{div}}(\Gamma) | \underline{\mathbf{v}}_h|_T \in \boldsymbol{RT}_0(T)\ \forall T\in\mathcal{T}_h\right\},$$

where $\boldsymbol{H}^0_{\mathrm{div}}(\Gamma)$ is defined in a standard manner

$$\boldsymbol{H}^0_{\mathrm{div}}(\Gamma) := \left\{\underline{\mathbf{v}}\in\boldsymbol{L}^2_t(\Gamma) | \mathrm{div}_\Gamma\underline{\mathbf{v}}\in L^2(\Gamma)\right\}.$$

Observe that the approximation space is conforming, i.e. $\boldsymbol{RT}_0\subset\boldsymbol{H}^0_{\mathrm{div}}(\Gamma)\subset\boldsymbol{H}^{-\frac{1}{2}}_{\mathrm{div}}(\Gamma)$. The Boundary Element Method then consists of seeking $\underline{\mathbf{J}}_h(\underline{\boldsymbol{\mu}})\in\boldsymbol{RT}_0$, for any fixed parameter value $\underline{\boldsymbol{\mu}}\in\boldsymbol{\mathcal{D}}$, such that

$$a(\underline{\mathbf{J}}_h(\underline{\boldsymbol{\mu}}),\underline{\mathbf{J}}_t;\underline{\boldsymbol{\mu}}) = f(\underline{\mathbf{J}}_t;\underline{\boldsymbol{\mu}}) \quad \forall\underline{\mathbf{J}}_t\in\boldsymbol{RT}_0. \tag{9}$$

4. Reduced basis method

The reduced basis method consists of approaching the "ideal" reduced basis, as described previously, by $\mathbb{W}_N = \mathrm{span}\{\underline{\mathbf{J}}_h(\underline{\boldsymbol{\mu}}_i)|i=1,\ldots,N\}$ for a set of carefully chosen parameters $\mathbb{S}_N = \{\underline{\boldsymbol{\mu}}_i\}_{i=1}^N$. The reduced basis approximation is defined by: for any $\underline{\boldsymbol{\mu}}\in D$, find $\underline{\mathbf{J}}_N(\underline{\boldsymbol{\mu}})\in\mathbb{W}_N$ such that

$$a(\underline{\mathbf{J}}_N(\underline{\boldsymbol{\mu}}),\underline{\mathbf{J}}_{N,t};\underline{\boldsymbol{\mu}}) = f(\underline{\mathbf{J}}_{N,t};\underline{\boldsymbol{\mu}}) \quad \forall\underline{\mathbf{J}}_{N,t}\in\mathbb{W}_N. \tag{10}$$

The following questions arise:

- How can $\mathbb{S}_N$ be chosen to get *accurate* approximations?
- How can problem (10) be solved in an *efficient* way?

They are discussed in the following sections.

Let us quickly introduce some notation: matrices and vector of size $\mathcal{N}\times\mathcal{N}$ resp. $\mathcal{N}$ are denoted in curly letters such as $\underline{\underline{\mathcal{A}}}$ and $\underline{b}$. The simple and double underlines stand for vectors resp. matrices. On the other hand, matrices and vectors independent of the dimension of the boundary element space $\mathcal{N}$ are denoted such as $\underline{\underline{\mathbf{A}}}$ and $\underline{\mathbf{b}}$.

Please cite this article in press as: M. Fares et al., The reduced basis method for the electric field integral equation, J. Comput. Phys. (2011), doi:10.1016/j.jcp.2011.03.023

```
Algorithm: RB-offline

  Algorithm1: Offline-procedure of the reduced basis method:the greedy algorithm to assemble the reduced basis space
  Input: Initial parameter value $\underline{\boldsymbol{\mu}}^1$
  Output: Reduced basis space $\mathbb{W}_N$ and associated parameter samples $\mathbb{S}_N$
  begin
    Set $\mathbb{S}_1 = \underline{\boldsymbol{\mu}}^1$ and $\mathbb{W}_1 = \mathrm{span}\{\underline{\mathbf{J}}_h(\underline{\boldsymbol{\mu}}^1)\}$ with $\underline{\mathbf{J}}_h(\underline{\boldsymbol{\mu}}^1)$, solution of (9) with $\underline{\boldsymbol{\mu}} = \underline{\boldsymbol{\mu}}^1$
    for $n = 2, \ldots, N$ do
      for each $\underline{\boldsymbol{\mu}} \in \Xi$ do
        Compute $\underline{\mathbf{J}}_{n-1}(\underline{\boldsymbol{\mu}}) \in \mathbb{W}_{n-1}$ solution of (10)
        Compute an error indicator $\eta(\underline{\boldsymbol{\mu}}) \approx \|\underline{\mathbf{J}}_h(\underline{\boldsymbol{\mu}}) - \underline{\mathbf{J}}_{n-1}(\underline{\boldsymbol{\mu}})\|_{\boldsymbol{H}_{\mathrm{div}}^{-\frac{1}{2}}(\Gamma)}$
      end
      Choose $\underline{\boldsymbol{\mu}}^n = \mathrm{argmax}_{\mu \in \Xi}\eta(\underline{\boldsymbol{\mu}})$
      $\mathbb{S}_n = \mathbb{S}_{n-1} \cup \underline{\boldsymbol{\mu}}^n$
      Compute the truth solution $\underline{\mathbf{J}}_h(\underline{\boldsymbol{\mu}}^n)$, solution of (9) with $\underline{\boldsymbol{\mu}} = \underline{\boldsymbol{\mu}}^n$
      $\mathbb{W}_n = \mathrm{span}\{\mathbb{W}_{n-1}, \underline{\mathbf{J}}_h(\underline{\boldsymbol{\mu}}^n)\}$
    end
  end
```

4.1. Accuracy

The question of accuracy of the reduced basis approximation is uniquely defined by the choice of the parameter sample space $\mathbb{S}_N$ and is determined using a greedy type algorithm, see [20,36] for an overview. Denote by Ξ some finite dimensional point-set of $\mathcal{D}$. The algorithm is illustrated in Algorithm 1.

Note that in the practical implementation, we use the residual of the linear system

$$\underline{\underline{A}}(\underline{\boldsymbol{\mu}})\underline{b}(\underline{\boldsymbol{\mu}}) = \underline{f}(\underline{\boldsymbol{\mu}}) \tag{11}$$

as an error indicator of $\|\underline{\mathbf{J}}_h(\underline{\boldsymbol{\mu}}) - \underline{\mathbf{J}}_n(\underline{\boldsymbol{\mu}})\|_{\boldsymbol{H}_{\mathrm{div}}^{-\frac{1}{2}}(\Gamma)}$. The matrix $\underline{\underline{A}}(\underline{\boldsymbol{\mu}})$ and vectors $\underline{f}(\underline{\boldsymbol{\mu}})$ resp. $\underline{b}(\underline{\boldsymbol{\mu}})$ denote the sesquilinear form $a(\cdot,\cdot;\underline{\boldsymbol{\mu}})$, the right hand side $f(\cdot;\underline{\boldsymbol{\mu}})$ and the solution $\underline{\mathbf{J}}_h(\underline{\boldsymbol{\mu}})$ expressed in the standard basis of $\boldsymbol{RT}_0$. This linear system represents the discrete variational problem (9), in the standard basis of $\boldsymbol{RT}_0$, defining the boundary element approximation for a given parameter value, i.e. the solution we are trying to approximate by the reduced basis method. It is called the *truth* approximation in the framework of Reduced Basis Methods.

More precisely, we choose the following quantity as an error estimation

$$\eta(\underline{\boldsymbol{\mu}}) = \frac{\|\underline{\underline{A}}(\underline{\boldsymbol{\mu}})\underline{b}^{rb}(\underline{\boldsymbol{\mu}}) - \underline{f}(\underline{\boldsymbol{\mu}})\|_{l^2}}{\max\limits_{\underline{\boldsymbol{\mu}} \in \Xi} \|\underline{f}(\underline{\boldsymbol{\mu}})\|_{l^2}}, \tag{12}$$

where $\underline{b}^{rb}(\underline{\boldsymbol{\mu}})$ represents the Reduced Basis approximation $\underline{\mathbf{J}}_n(\underline{\boldsymbol{\mu}})$ in the standard basis of $\boldsymbol{RT}_0$. Note that due to the equivalence of norms on finite dimensional spaces the $\|\cdot\|_{l_2}$-norm of the degrees of freedom is equivalent to the $\|\cdot\|_{L_2}$-norm of the corresponding functions which itself is equivalent to the natural $\|\cdot\|_{\boldsymbol{H}_{\mathrm{div}}^{-\frac{1}{2}}(\Gamma)}$-norm. However, depending on the regularity of the underlying function the scaling in the mesh size $\mathtt{h}$ might be different. But since we only consider discrete functions, they are sufficiently regular and the scaling in the mesh size $\mathtt{h}$ (which does not change at any instance) is the same.

Remark 4.1. For the purpose of well-conditioned systems we use the Gram–Schmidt process to orthonormalize the basis functions of $\mathbb{W}_N$.

The previously defined algorithm identifies the reduced basis space $\mathbb{W}_N$ such that $\mathbb{W}_N$ is a good approximation to $\mathcal{M}_h$. In practice, exponential convergence is observed with respect to N, as the numerical results presented in Section 6 will show.

4.2. Efficiency

Once the reduced basis space is assembled, the goal is to efficiently solve the *input–output* procedure:

Please cite this article in press as: M. Fares et al., The reduced basis method for the electric field integral equation, J. Comput. Phys. (2011), doi:10.1016/j.jcp.2011.03.023

```
Algorithm: RB-offline

    Input: A parameter value $\underline{\boldsymbol{\mu}}$ and a discrete set of directions $D$
    Output: The Radar Cross Section RCS($\underline{\mathbf{J}}_N(\underline{\boldsymbol{\mu}}), \hat{\underline{\mathbf{d}}}$) of the reduced basis approximation
    $\underline{\mathbf{J}}_N(\underline{\boldsymbol{\mu}}) \in \mathbb{W}_N$ for all directions $\hat{\underline{\mathbf{d}}} \in D$
```

The previous input–output procedure can be in a many-query context, in the framework for an optimization problem or shape recognition problem, for example. Note that if we do not manage to solve problem (10) efficiently, there is no need for the reduced basis approximation since the solution could be obtained through a full BEM-approximation using (9). Observe that solving (9) depends on the dimension $\mathcal{N}$ of the approximation space $\boldsymbol{RT}_0$. We therefore define *efficiency* in the sense that the solution of (10) should be independent of $\mathcal{N}$.

That the following assumption is satisfied exactly or approximately:

Assumption 4.2 (*Affine decomposition*). The sesquilinear form a and the linear forms f, $\underline{\mathbf{s}}_\infty$ can be decomposed into a finite sum of parameter dependent scalar functions multiplied by parameter-independent forms, i.e.

$$a(\underline{\mathbf{w}}, \underline{\mathbf{v}}; k) = \sum_{m=1}^{M_k} \Theta^m(k) a^m(\underline{\mathbf{w}}, \underline{\mathbf{v}}),$$

$$f(\underline{\mathbf{v}}; \underline{\boldsymbol{\mu}}) = \sum_{m=1}^{M_f} \underline{\boldsymbol{\Theta}}_f^m(\underline{\boldsymbol{\mu}}) \cdot \underline{\mathbf{f}}^m(\underline{\mathbf{v}}),$$

$$\underline{\mathbf{s}}_\infty(\underline{\mathbf{v}}; k, \hat{\underline{\mathbf{d}}}) = \hat{\underline{\mathbf{d}}} \times \left(\sum_{m=1}^{M_\infty} \Theta_\infty^m(k, \hat{\underline{\mathbf{d}}}) \underline{\mathbf{s}}^m(\underline{\mathbf{v}}) \times \hat{\underline{\mathbf{d}}} \right),$$

with

$$\Theta^m : \mathbb{R} \to \mathbb{C}, \quad a^m : \boldsymbol{RT}_0 \times \boldsymbol{RT}_0 \to \mathbb{C}$$

$$\underline{\boldsymbol{\Theta}}_f^m : \boldsymbol{\mathcal{D}} \to \mathbb{C}^3, \quad \underline{\mathbf{f}}^m : \boldsymbol{RT}_0 \to \mathbb{C}^3$$

$$\Theta_\infty^m : \boldsymbol{\mathcal{D}} \to \mathbb{C}, \quad \underline{\mathbf{s}}^m : \boldsymbol{RT}_0 \to \mathbb{C}^3.$$

Remark 4.3. Note that in the case of the parametrized EFIE, this assumption is not obvious. On the contrary, without any additional tools the assumption is not satisfied exactly, i.e. the simultaneous presence of the variable and the parameter in the power of the exponential function of the forms

$$a(\underline{\mathbf{J}}, \underline{\mathbf{J}}_t; k) = ikZ \int_\Gamma \int_\Gamma \frac{e^{ik|\underline{\mathbf{x}}-\underline{\mathbf{y}}|}}{4\pi|\underline{\mathbf{x}}-\underline{\mathbf{y}}|} \left\{ \underline{\mathbf{J}}(\underline{\mathbf{x}}) \cdot \overline{\underline{\mathbf{J}}_t(\underline{\mathbf{y}})} - \frac{1}{k^2} \mathrm{div}_{\Gamma,x} \underline{\mathbf{J}}(\underline{\mathbf{x}}) \mathrm{div}_{\Gamma,y} \overline{\underline{\mathbf{J}}_t(\underline{\mathbf{y}})} \right\} \underline{\mathbf{dx}}\, \underline{\mathbf{dy}},$$

$$f(\underline{\mathbf{J}}_t; \underline{\boldsymbol{\mu}}) = -\int_\Gamma e^{ik\hat{\underline{\mathbf{k}}}\cdot\underline{\mathbf{y}}} \underline{\mathbf{p}} \cdot \overline{\underline{\mathbf{J}}_t(\underline{\mathbf{y}})} \underline{\mathbf{dy}},$$

$$\underline{\mathbf{s}}_\infty(\underline{\mathbf{J}}; k, \hat{\underline{\mathbf{d}}}) = \frac{ikZ}{4\pi} \hat{\underline{\mathbf{d}}} \times \left(\int_\Gamma \underline{\mathbf{J}}(\underline{\mathbf{x}}) e^{ik\underline{\mathbf{x}}\cdot\hat{\underline{\mathbf{d}}}} \underline{\mathbf{dx}} \times \hat{\underline{\mathbf{d}}} \right)$$

yields complications. A way to achieve the affine decomposition in an approximative manner is discussed in Section 5.

This particular assumption is motivated by the fact that the forms, which depend on the dimension $\mathcal{N}$ of the boundary element space, can be precomputed for the basis functions of the reduced basis space $\mathbb{W}_N$. The slight differences between scalar and vector quantities is due to the tools used to recover this decomposition and is discussed in details in Section 5. We therefore postpone the discussion of how to get this decomposition and suppose for now that this assumption holds.

Given $\mathbb{W}_N = \mathrm{span}\{\underline{\xi}_i | i = 1, \ldots, N\}$, for any $N \geqslant 1$, we then pre-assemble in an offline procedure the M corresponding matrices $\underline{\underline{\mathbf{A}}}^m \in \mathbb{C}^{N,N}, \underline{\underline{\mathbf{F}}}^m, \underline{\underline{\mathbf{S}}}^m \in \mathbb{C}^{N,3}$ to the forms a^m, $\underline{\mathbf{f}}^m$ and $\underline{\mathbf{s}}^m$ defined by

$$\underline{\underline{\mathbf{A}}}_{i,j}^m = a^m(\underline{\xi}_j, \underline{\xi}_i), \quad 1 \leqslant i,j \leqslant N,\ 1 \leqslant m \leqslant M_k,$$

$$\underline{\underline{\mathbf{F}}}_{i,j}^m = \underline{\mathbf{f}}_j^m(\underline{\xi}_i), \quad 1 \leqslant i \leqslant N,\ 1 \leqslant j \leqslant 3,\ 1 \leqslant m \leqslant M_f,$$

$$\underline{\underline{\mathbf{S}}}_{i,j}^m = \underline{\mathbf{s}}_j^m(\underline{\xi}_i), \quad 1 \leqslant i \leqslant N,\ 1 \leqslant j \leqslant 3,\ 1 \leqslant m \leqslant M_\infty.$$

Note that this assembling depends on $\mathcal{N}$, but once the matrices are assembled they are of dimension $N \times N$ resp. $N \times 3$, thus independent on $\mathcal{N}$.

In a similar way we pre-compute quantities related to the residual of the linear system (11), namely the matrices $\underline{\underline{\mathbf{R_1}}}^{m,n} \in \mathbb{C}^{N,N}$, $\underline{\mathbf{R_2}}^{m,n} \in \mathbb{C}^{3,N}$ and $R_3^{m,n} \in \mathbb{C}^{3,3}$.

$$\underline{\underline{\mathbf{R_1}}}_{i,j}^{m,n} = (\underline{\underline{\mathcal{A}}}^m \hat{\underline{\xi}}_j)^* \underline{\underline{\mathcal{A}}}^n \hat{\underline{\xi}}_i, \quad 1 \leqslant i,\ j \leqslant N,\ 1 \leqslant m,n \leqslant M_k,$$

$$\underline{\mathbf{R_2}}_i^{m,n} = (\underline{f}^m)^* \underline{\underline{\mathcal{A}}}^n \hat{\underline{\xi}}_i, \quad 1 \leqslant i \leqslant N,\ 1 \leqslant m \leqslant M_k,\ 1 \leqslant n \leqslant M_f,$$

$$R_3^{m,n} = (\underline{f}^m)^* \underline{f}^n, \quad 1 \leqslant m,\ n \leqslant M_f,$$

Please cite this article in press as: M. Fares et al., The reduced basis method for the electric field integral equation, J. Comput. Phys. (2011), doi:10.1016/j.jcp.2011.03.023

where $\underline{\underline{\mathcal{A}}}^m \in \mathbb{C}^{\mathcal{N},\mathcal{N}}$,$\underline{f}^m \in \mathbb{C}^{\mathcal{N},3}$ and $\hat{\underline{\xi}}_i \in \mathbb{C}^{\mathcal{N}}$ denote the vectorial representation of the sesquilinear forms $a^m(\cdot,\cdot)$, linear forms $\mathbf{f}^m(\cdot)$ and basis functions $\underline{\xi}_i$ in the standard basis of $\boldsymbol{RT}_0$.

Once this pre-assembling is completed during the *online* stage of the algorithm, the previously described Input–Output procedure can be solved in a fast way, as described in Algorithm 2.

Remark 4.4 (*Costs*). It shall be noted that the notion of complexity is of two "dimensions". The first one concerns the mesh size of the discretized surface and the corresponding Boundary Element Space. During the *Offline* algorithm, for solving each new snapshot, the number of degrees of freedom $\mathcal{N}$ of the mesh will be decisive for the computing time. For an efficient solver one can use the Fast-Multipole technique developed by Greengard and Rokhlin [15] which results in $\mathcal{N}\log(\mathcal{N})$ operations. On the other hand for large or high dimensional parameter spaces, the search over the train sample Ξ in Algorithm 1 becomes time limiting and depending linearly on the number of points in the discrete set Ξ. There can be an implicit connection between those two dimensions through the highest wave number considered in the parameter space, which dictates a certain fineness of the mesh in order to get an accurate truth solution for all parameter values.

During the *Online* stage however, the computing time no longer depends on $\mathcal{N}$ and solely depends on N, M_k, M_f, M_∞ and the number of directions in the set D.

```
Algorithm: RB-online

    Algorithm 2: Online-procedure of the reduced basis method
    Input:A parameter value $\underline{\boldsymbol{\mu}}$ and a discrete set of directions $D$
    Output: The Radar Cross Section RCS($\underline{\mathbf{J}}_N(\underline{\boldsymbol{\mu}}), \hat{\underline{\mathbf{d}}}$) of the reduced basis approximation $\underline{\mathbf{J}}_N(\underline{\boldsymbol{\mu}}) \in \mathbb{W}_N$ for the given directions
    $\hat{\underline{\mathbf{d}}} \in D$
    begin
        (i) Assemble the matrix $\underline{\underline{\mathbf{A}}}^{rb}(\underline{\boldsymbol{\mu}}) \in \mathbb{C}^{N\times N}$ and vector $\underline{\mathbf{F}}^{rb}(\underline{\boldsymbol{\mu}}) \in \mathbb{C}^N$ as

        $\underline{\underline{\mathbf{A}}}^{rb}(\underline{\boldsymbol{\mu}}) = \sum_{m=1}^{M} \Theta^m(\underline{\boldsymbol{\mu}})\underline{\underline{\mathbf{A}}}^m$   and $\underline{\mathbf{F}}^{rb}(\underline{\boldsymbol{\mu}}) = \sum_{m=1}^{M_f} \underline{\underline{\mathbf{F}}}^m \underline{\boldsymbol{\Theta}}_f^m(\underline{\boldsymbol{\mu}})$.

        (ii) Solve the linear system $\underline{\underline{\mathbf{A}}}^{rb}(\underline{\boldsymbol{\mu}})\underline{\mathbf{b}}(\underline{\boldsymbol{\mu}}) = \underline{\mathbf{F}}^{rb}(\underline{\boldsymbol{\mu}})$.
        /*The reduced basis solution is then given by

        $\underline{\mathbf{J}}_N(\underline{\boldsymbol{\mu}}) = \sum_{i=1}^{N} (\underline{\mathbf{b}}(\underline{\boldsymbol{\mu}}))_i \underline{\xi}_i$.

                                    */
        (iii) for each $\hat{\underline{\mathbf{d}}} \in D$ do
            Compute the RCS signal

        RCS($\underline{\mathbf{J}}_N(\underline{\boldsymbol{\mu}}); k, \hat{\underline{\mathbf{d}}}$) $= 10\log_{10}\left(4\pi \frac{|\underline{\mathbf{s}}_\infty(\hat{\underline{\mathbf{d}}})|^2}{|\underline{\mathbf{E}}^{inc}(\underline{\boldsymbol{\mu}})|^2}\right)$

            with $\underline{\mathbf{s}}_\infty(\hat{\underline{\mathbf{d}}}) := \sum_{i=1}^{N}\sum_{m=1}^{M_\infty} b_i(\underline{\boldsymbol{\mu}})\Theta_\infty^m(k, \hat{\underline{\mathbf{d}}})\hat{\underline{\mathbf{d}}} \times (\underline{\mathbf{s}}_i^m \times \hat{\underline{\mathbf{d}}})$ where $\underline{\mathbf{s}}_i^m \in \mathbb{C}^3$ is the i-th row of the matrix $\underline{\underline{\mathbf{S}}}^m$.
        end
        (iv) Compute the error indication:

        $\eta(\underline{\boldsymbol{\mu}}) = \frac{\sqrt{\eta_1(\underline{\boldsymbol{\mu}}) - 2\eta_2(\underline{\boldsymbol{\mu}}) + \eta_3(\underline{\boldsymbol{\mu}})}}{\max_{\underline{\boldsymbol{\mu}} \in \Xi} \|F(\underline{\boldsymbol{\mu}})\|_{l^2}}$.

    with

        $\eta_1(\underline{\boldsymbol{\mu}}) = \sum_{m,n=1}^{M_k} \left(\underline{\mathbf{b}}(\underline{\boldsymbol{\mu}})\Theta^m(\underline{\boldsymbol{\mu}})\right)^* \underline{\underline{\mathbf{R_1}}}^{m,n}\underline{\mathbf{b}}(\underline{\boldsymbol{\mu}})\Theta^n(\underline{\boldsymbol{\mu}})$

        $\eta_2(\underline{\boldsymbol{\mu}}) = \sum_{m=1}^{M_k}\sum_{n=1}^{M_f} \left(\underline{\boldsymbol{\Theta}}_f^m(\underline{\boldsymbol{\mu}})\right)^* \underline{\underline{\mathbf{R_2}}}^{m,n}\underline{\mathbf{b}}(\underline{\boldsymbol{\mu}})\Theta^n(\underline{\boldsymbol{\mu}})$

        $\eta_3(\underline{\boldsymbol{\mu}}) = \sum_{m,n=1}^{M_f} \left(\underline{\boldsymbol{\Theta}}_f^m(\underline{\boldsymbol{\mu}})\right)^* R_3^{m,n}\underline{\boldsymbol{\Theta}}_f^n(\underline{\boldsymbol{\mu}})$

    end
```

Please cite this article in press as: M. Fares et al., The reduced basis method for the electric field integral equation, J. Comput. Phys. (2011), doi:10.1016/j.jcp.2011.03.023

5. Empirical interpolation method

This section is devoted to finding strategies to satisfy the affine assumption approximatively. The Empirical Interpolation Method (EIM) [3,16,23], also called Magic Points, is frequently used in the framework of reduced basis methods. A similar but alternative approach is presented in [26] where the interpolation points are chosen in a different manner. We first introduce the method and show some numerical examples that are essential in our context. In a second part we will generalize the existing method to better fit the needs in the framework of the parametrized EFIE.

5.1. Empirical interpolation method

Consider a function $f : \Omega \times \boldsymbol{\mathcal{D}} \to \mathbb{C}$ that is smooth enough, i.e. $f(\cdot, \underline{\boldsymbol{\mu}}) \in C^0(\overline{\Omega})$ for all $\underline{\boldsymbol{\mu}} \in \boldsymbol{\mathcal{D}}$. Note that the parameter domain is not necessarily the same as the one for the reduced basis method. When combining the EIM with the reduced basis method, it also consists of a subset of the parameter space given by the underlying parametrized problem. The EIM provides a set of parameter values $\mathbb{I}_M = \{\underline{\boldsymbol{\mu}}_j\}_{j=1}^M$ and basis functions $\mathbb{Q}_M = \{q_j\}_{j=1}^M$ such that the interpolant defined by

$$\mathcal{I}_M(f)(\underline{\mathbf{x}}; \underline{\boldsymbol{\mu}}) := \sum_{j=1}^{M} \alpha_j(\underline{\boldsymbol{\mu}}) q_j(\underline{\mathbf{x}}) \tag{13}$$

is an approximation of $f(\underline{\mathbf{x}}; \underline{\boldsymbol{\mu}})$ for all $(\underline{\mathbf{x}}; \underline{\boldsymbol{\mu}}) \in \Omega \times \boldsymbol{\mathcal{D}}$ and where the coefficients $\{\alpha_j(\underline{\boldsymbol{\mu}})\}_{j=1}^M$ are obtained by solving a lower triangular linear system of size M. Indeed, the interpolant can be chosen to be arbitrarily accurate depending on the number of modes M used. The accuracy is measured in the $L^\infty(\Omega \times \boldsymbol{\mathcal{D}})$-norm. In practice, exponential convergence is observed with respect to the number of modes, see the following section of numerical results of the EIM. The EIM also uses a greedy algorithm to pick the parameters $\mathbb{I}_M = \{\underline{\boldsymbol{\mu}}_j\}_{j=1}^M$ and is given in Algorithm 3.

The algorithm `EIM` uses the module `ERROR` which is described in Algorithm 4 and computes the next basis function and interpolation point for a given system of basis functions and interpolation points.

Indeed, for any new parameter value $\underline{\boldsymbol{\mu}}$ the parameter dependent coefficients $\{\alpha_j(\underline{\boldsymbol{\mu}})\}_{j=1}^M$ are obtained by solving the following linear system

$$\sum_{j=1}^{M} \underline{\underline{\mathbf{B}}}_{ij}^M \alpha_j(\underline{\boldsymbol{\mu}}) = f(\underline{\mathbf{x}}_i; \underline{\boldsymbol{\mu}}), \quad 1 \leqslant i \leqslant M,$$

where the interpolation matrix $\underline{\underline{\mathbf{B}}}^M$ is defined by $\underline{\underline{\mathbf{B}}}_{ij}^M = q_j(\underline{\mathbf{x}}_i)$ and where $\mathbb{T}_M = \{\underline{\mathbf{x}}_i\}_{j=1}^M$ are the interpolation points provided by the EIM.

Algorithm: `EIM`

```
Algorithm 3: The Empirical Interpolation Method
Input: Function $f$, $\Omega$, $\boldsymbol{\mathcal{D}}$, $M$
/*$f : \Omega \times \boldsymbol{\mathcal{D}} \to \mathbb{C}$: function to be interpolated*/
/*$M$: Maximal length of expansion*/
Output: Parameter samples $\mathbb{I}_M = \{\underline{\boldsymbol{\mu}}_j\}_{j=1}^M$, interpolation points $\mathbb{T}_M = \{\underline{\mathbf{x}}_j\}_{j=1}^M$,
basis functions $\mathbb{Q}_M = \{q_j\}_{j=1}^M$ and interpolation error Err
begin
  Set $\Xi \subset \boldsymbol{\mathcal{D}}$, a finite dimensional point-set and fine enough
  $B^0 = \mathbb{Q}_0 = \mathbb{I}_0 = \mathbb{T}_0 = \emptyset$
  for $m = 1,\ldots,M$ do
    /*Get m-th basis function and m-th interpolation point*/
    $(\mathrm{Err}_m, q_m, \underline{\boldsymbol{\mu}}_m, \underline{\mathbf{x}}_m) \leftarrow$ ERROR$(\mathbb{T}_{m-1}, \mathbb{Q}_{m-1}, m-1)$
    Set $\mathbb{Q}_m = \mathbb{Q}_{m-1} \cup \{q_m\}$, $\mathbb{I}_m = \mathbb{I}_{m-1} \cup \{\underline{\boldsymbol{\mu}}_m\}$, $\mathbb{T}_m = \mathbb{T}_{m-1} \cup \{\underline{\mathbf{x}}_m\}$
  end
    $(\mathrm{Err}, \cdot) \leftarrow$ ERROR$(\mathbb{T}_M, \mathbb{Q}_M, M)$
end
```

Remark 5.1. Note that the sample space from the Empirical Interpolation Method $\mathbb{I}_M$ is not to be mistaken for the sample space $\mathbb{S}_M$ of the reduced basis method. The former one is linked to a good approximation of the interpolant defined by (13). The latter one defines the reduced basis and therefore also accounts for phenomena arising from the physical problem.

Please cite this article in press as: M. Fares et al., The reduced basis method for the electric field integral equation, J. Comput. Phys. (2011), doi:10.1016/j.jcp.2011.03.023

In order to satisfy the affine decomposition, Assumption 4.2, we use the Empirical Interpolation Method, as pointed out in Remark 4.3. The following examples show how this method is involved to used the affine decomposition assumption in the framework of the parametrized EFIE.

Example 5.2 (*Kernel function*). The kernel function G_k is first split into a parameter independent singular part and a parameter dependent non-singular part

$$G(r;k) = \frac{1}{4\pi r} + G_{ns}(r;k) \quad \text{with} \quad G_{ns}(r;k) = \frac{e^{ikr}-1}{4\pi r}.$$

This splitting is due to the underlying boundary element discretization which requires different numerical integration for the sesquilinear forms of those two parts. Next, the Empirical Interpolation Method is used to construct an interpolant

$$\mathcal{I}_M(G_{ns})(r;k) := \sum_{m=1}^{M_g} \alpha^g_m(k) q^g_m(r).$$

```
Algorithm: ERROR

Algorithm 4: The ERROR module
Input: $\mathbb{T}_m, \mathbb{Q}_m, m$
Output: Error of interpolation Err, next basis function $\tilde{q}$, parameter value $\underline{\tilde{\boldsymbol{\mu}}}$ and point $\underline{\tilde{\mathbf{x}}}$ that yield the maximum.
begin
    Define the interpolation matrix by
        $\underline{\underline{\mathbf{B}}}^m_{ij} = q_j(\underline{\mathbf{x}}_i), \qquad 1 \leqslant i,j \leqslant m.$
    for each $\underline{\mu} \in \Xi$ do
        Solve the linear system
            $\sum_{j=1}^{m} \underline{\underline{\mathbf{B}}}^m_{ij} f_j(\underline{\boldsymbol{\mu}}) = f(\underline{\mathbf{x}}_i; \underline{\boldsymbol{\mu}}), \qquad 1 \leqslant i \leqslant m, \underline{\mathbf{x}}_i \in \mathbb{T}_m.$
        Compute the interpolant defined by
            $\mathcal{I}_m(f)(\underline{\mathbf{x}}; \underline{\boldsymbol{\mu}}) = \sum_{j=1}^{m} f_j(\underline{\boldsymbol{\mu}}) q_j(\underline{\mathbf{x}}), \qquad q_j \in \mathbb{Q}_m.$
        Compute the error function
            $e(\underline{\mathbf{x}}; \underline{\boldsymbol{\mu}}) = f(\underline{\mathbf{x}}; \underline{\boldsymbol{\mu}}) - \mathcal{I}_m(f)(\underline{\mathbf{x}}; \underline{\boldsymbol{\mu}})$
        and the interpolation error
            $\eta(\underline{\boldsymbol{\mu}}) = \|e(\cdot; \underline{\boldsymbol{\mu}})\|_{L^\infty(\Omega)}.$
    end
    Set $\underline{\tilde{\boldsymbol{\mu}}} = \mathrm{argmax}_{\mu \in \Xi} \eta(\underline{\boldsymbol{\mu}})$, $\underline{\tilde{\mathbf{x}}} = \mathrm{argsup}_{\underline{\mathbf{x}} \in \Omega} |e(\underline{\mathbf{x}}, \underline{\tilde{\boldsymbol{\mu}}})|$, $\tilde{q} = e(\cdot, \underline{\tilde{\boldsymbol{\mu}}}) / e(\underline{\tilde{\mathbf{x}}}, \underline{\tilde{\boldsymbol{\mu}}})$ and Err $= \eta(\underline{\tilde{\boldsymbol{\mu}}})$
end
```

Replacing $G_{ns}(r;k)$ by its interpolant $\mathcal{I}_M(G_{ns})(r;k)$ in the sesquilinear form a yields

$$\begin{aligned} a(\underline{\mathbf{J}}, \underline{\mathbf{J}}_t; k) \approx{}& \frac{ikZ}{4\pi} \int_\Gamma \int_\Gamma \frac{1}{r} \underline{\mathbf{J}}(\underline{\mathbf{x}}) \cdot \overline{\underline{\mathbf{J}}_t(\underline{\mathbf{y}})}\, \underline{\mathbf{dx}}\underline{\mathbf{dy}} - \frac{iZ}{4\pi k} \int_\Gamma \int_\Gamma \frac{1}{r} \mathrm{div}_{\Gamma,x} \underline{\mathbf{J}}(\underline{\mathbf{x}}) \mathrm{div}_{\Gamma,y} \overline{\underline{\mathbf{J}}_t(\underline{\mathbf{y}})}\, \underline{\mathbf{dx}}\underline{\mathbf{dy}} + \sum_{m=1}^{M_g} ikZ \alpha^g_m(k) \int_\Gamma \int_\Gamma q^g_m(r) \underline{\mathbf{J}}(\underline{\mathbf{x}}) \\ & \cdot \overline{\underline{\mathbf{J}}_t(\underline{\mathbf{y}})}\, \underline{\mathbf{dx}}\underline{\mathbf{dy}} - \sum_{m=1}^{M_g} \frac{iZ}{k} \alpha^g_m(k) \int_\Gamma \int_\Gamma q^g_m(r) \mathrm{div}_{\Gamma,x} \underline{\mathbf{J}}(\underline{\mathbf{x}}) \mathrm{div}_{\Gamma,y} \overline{\underline{\mathbf{J}}_t(\underline{\mathbf{y}})}\, \underline{\mathbf{dx}}\underline{\mathbf{dy}}, \end{aligned}$$

where $r = |\underline{\mathbf{x}} - \underline{\mathbf{y}}|$. Since the interpolant can be constructed to any precision (point-wise over the spatial and parameter domains), it is reasonable to use the approximate sesquilinear form. We define

Please cite this article in press as: M. Fares et al., The reduced basis method for the electric field integral equation, J. Comput. Phys. (2011), doi:10.1016/j.jcp.2011.03.023

$$\Theta^m(k)=\begin{cases}\frac{ikZ}{4\pi} & \text{if } m=1,\\ -\frac{iZ}{4\pi k} & \text{if } m=2,\\ ikZ\alpha_m^g(k) & \text{if } 3\leqslant m\leqslant 2+M_g,\\ -\frac{iZ}{k}\alpha_m^g(k) & \text{if } 3+M_g\leqslant m\leqslant 2+2M_g\end{cases}$$

for all $1\leqslant m\leqslant M_{\mathrm{k}}=2M_g+2$. In the same manner we define the parameter independent forms by

$$a^m(\underline{\mathbf{w}},\underline{\mathbf{v}})=\begin{cases}\int_\Gamma\int_\Gamma \frac{1}{r}\underline{\mathbf{w}}(\underline{\mathbf{x}})\cdot\overline{\underline{\mathbf{v}}(\underline{\mathbf{y}})}\underline{\mathbf{dx}}\underline{\mathbf{dy}} & \text{if } m=1,\\ \int_\Gamma\int_\Gamma \frac{1}{r}\mathrm{div}_{\Gamma,x}\underline{\mathbf{w}}(\underline{\mathbf{x}})\mathrm{div}_{\Gamma,y}\overline{\underline{\mathbf{v}}(\underline{\mathbf{y}})}\underline{\mathbf{dx}}\underline{\mathbf{dy}} & \text{if } m=2,\\ \int_\Gamma\int_\Gamma q_m^g(r)\underline{\mathbf{w}}(\underline{\mathbf{x}})\cdot\overline{\underline{\mathbf{v}}(\underline{\mathbf{y}})}\underline{\mathbf{dx}}\underline{\mathbf{dy}} & \text{if } 3\leqslant m\leqslant 2+M_g,\\ \int_\Gamma\int_\Gamma q_m^g(r)\mathrm{div}_{\Gamma,x}\underline{\mathbf{w}}(\underline{\mathbf{x}})\mathrm{div}_{\Gamma,y}\overline{\underline{\mathbf{v}}(\underline{\mathbf{y}})}\underline{\mathbf{dx}}\underline{\mathbf{dy}} & \text{if } 3+M_g\leqslant m\leqslant 2+2M_g.\end{cases}$$

Example 5.3 (*Trace of incident plane wave*). The second example deals with the trace of the incident plane wave $\underline{\mathbf{E}}^{inc}(\underline{\mathbf{x}};\underline{\boldsymbol{\mu}})=-\underline{\mathbf{p}}e^{ik\hat{\underline{\mathbf{k}}}\cdot\underline{\mathbf{x}}}$ onto Γ. Observe that since we integrate $\underline{\mathbf{E}}^{inc}$ against a tangential test function $\underline{\mathbf{J}}_t$ we do not have to project $\mathbf{E}^{inc}$ onto the surface Γ. Thus we can write

$$f(\underline{\mathbf{J}}_t;\underline{\boldsymbol{\mu}})=-\underline{\mathbf{p}}\cdot\int_\Gamma e^{ik\hat{\underline{\mathbf{k}}}\cdot\underline{\mathbf{y}}}\overline{\underline{\mathbf{J}}_t(\underline{\mathbf{y}})}\underline{\mathbf{dy}}$$

and observe that the integral still depends on the parameters k and $\hat{\underline{\mathbf{k}}}$. We therefore apply the Empirical Interpolation Method to the scalar function $f_e(\underline{\mathbf{x}};k,\hat{\underline{\mathbf{k}}})=e^{ik\hat{\underline{\mathbf{k}}}\cdot\underline{\mathbf{x}}}$ which results in a set of basis functions $\{q_m^f\}_{m=1}^{M_f}$ that defines the interpolant

$$\mathcal{I}_M(f_e)(\underline{\mathbf{x}};k,\hat{\underline{\mathbf{k}}})=\sum_{m=1}^{M_f}\alpha_m^f(k,\hat{\underline{\mathbf{k}}})q_m^f(\underline{\mathbf{x}}).$$

Again, the coefficients $\{\alpha_m^f(k,\hat{\underline{\mathbf{k}}})\}_{m=1}^{M_f}$ can be obtained by solving a linear system of size M_f for any new parameter values. Finally we can write

$$f(\underline{\mathbf{J}}_t;\underline{\boldsymbol{\mu}})\approx-\sum_{m=1}^{M_f}\alpha_m^f(k,\hat{\underline{\mathbf{k}}})\underline{\mathbf{p}}\cdot\int_\Gamma q_m^f(\underline{\mathbf{y}})\overline{\underline{\mathbf{J}}_t(\underline{\mathbf{y}})}\underline{\mathbf{dy}}.$$

We finally define $\underline{\boldsymbol{\Theta}}_f^m(\underline{\boldsymbol{\mu}})=-\alpha_m^f(k,\hat{\underline{\mathbf{k}}})\underline{\mathbf{p}}$ and $\underline{\mathbf{f}}^m=\int_\Gamma q_m^f(\underline{\mathbf{y}})\overline{\underline{\mathbf{J}}_t(\underline{\mathbf{y}})}\underline{\mathbf{dy}}$.

Example 5.4 (*Radar Cross Section*). The third example treats the non-affine character of the functional

$$\underline{\mathbf{s}}_\infty(\underline{\mathbf{J}};k,\hat{\underline{\mathbf{d}}})=\frac{ikZ}{4\pi}\hat{\underline{\mathbf{d}}}\times\left(\int_\Gamma\underline{\mathbf{J}}(\underline{\mathbf{x}})e^{ik\underline{\mathbf{x}}\cdot\hat{\underline{\mathbf{d}}}}\underline{\mathbf{dx}}\times\hat{\underline{\mathbf{d}}}\right)$$

needed to compute the RCS-signature in a given direction $\hat{\underline{\mathbf{d}}}$ for a current $\underline{\mathbf{J}}$. The non-affine behavior lies in the function $e^{ik\underline{\mathbf{x}}\cdot\hat{\underline{\mathbf{d}}}}$. We therefore apply the EIM to the function $f_e(\underline{\mathbf{x}};k,\hat{\underline{\mathbf{d}}})=e^{ik\underline{\mathbf{x}}\cdot\hat{\underline{\mathbf{d}}}}$. Observe that this is the same function as in the previous example, but for a different parameter domain. We therefore compute the interpolant twice to keep the number of necessary modes M as low as possible. Again, the EIM results in a set of basis functions $\{q_m^\infty\}_{m=1}^{M_\infty}$ and efficiently computable coefficients $\{\alpha_m^\infty(k,\hat{\underline{\mathbf{k}}})\}_{m=1}^{M_f}$ for each new parameter values. We can then write

$$\underline{\mathbf{s}}_\infty(\underline{\mathbf{J}};k,\hat{\underline{\mathbf{d}}})\approx\hat{\underline{\mathbf{d}}}\times\left(\left(\sum_{m=1}^{M_\infty}\frac{ikZ}{4\pi}\alpha_m^\infty(k,\hat{\underline{\mathbf{d}}})\int_\Gamma\underline{\mathbf{J}}(\underline{\mathbf{x}})q_m^\infty(\underline{\mathbf{x}})\underline{\mathbf{dx}}\right)\times\hat{\underline{\mathbf{d}}}\right)$$

and we define $\Theta_\infty^m(k,\hat{\underline{\mathbf{d}}})=\frac{ikZ}{4\pi}\alpha_m^\infty(k,\hat{\underline{\mathbf{d}}})$ and $\underline{\mathbf{s}}^m=\int_\Gamma\underline{\mathbf{J}}(\underline{\mathbf{x}})q_m^\infty(\underline{\mathbf{x}})\underline{\mathbf{dx}}$.

5.1.1. Numerical results

Let us test the approximation and convergence properties of the Empirical Interpolation Method. We will consider four test cases given by:

	Function	Parameter	$\mathcal{D}$	Fixed values	Spatial domain
i	$f(r;k)=\frac{e^{ikr}-1}{r}$	k	$[1,k_{\max}]$		$r\in(0,R_{\max})$
ii	$f(\underline{\mathbf{x}};\theta)=e^{ik\hat{\underline{\mathbf{k}}}(\theta,\varphi)\cdot\underline{\mathbf{x}}}$	θ	$[0,\pi]$	k, $\varphi=0$	$\underline{\mathbf{x}}\in\Gamma$
iii	$f(\underline{\mathbf{x}};\theta,\varphi)=e^{ik\hat{\underline{\mathbf{k}}}(\theta,\varphi)\cdot\underline{\mathbf{x}}}$	θ, φ	$[0,\pi]\times[0,2\pi)$	k	$\underline{\mathbf{x}}\in\Gamma$
iv	$f(\underline{\mathbf{x}};k,\theta)=e^{ik\hat{\underline{\mathbf{k}}}(\theta,\varphi)\cdot\underline{\mathbf{x}}}$	k, θ	$[0,k_{max}]\times[0,\pi]$	$\varphi=0$	$\underline{\mathbf{x}}\in\Gamma$

Please cite this article in press as: M. Fares et al., The reduced basis method for the electric field integral equation, J. Comput. Phys. (2011), doi:10.1016/j.jcp.2011.03.023

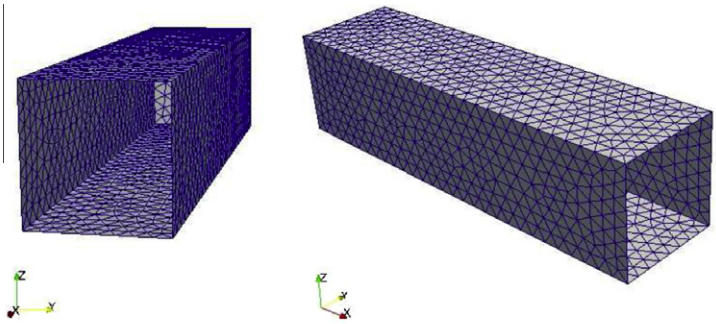

Fig. 3. Two different views on the surface Γ used for the test cases (ii), (iii) and (iv).

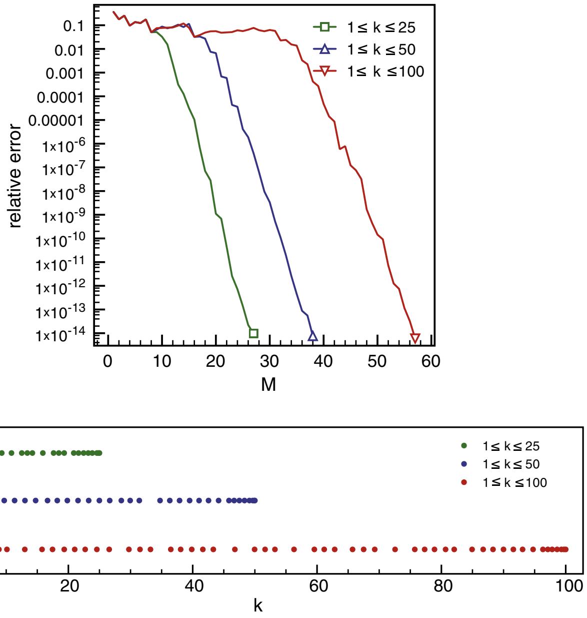

Fig. 4. Relative error in the test case (i) for different values of $k_{\max}$ depending on the length M of the expansion (top) and the corresponding picked parameter values (bottom).

We recall that the wave direction $\underline{\hat{\mathbf{k}}}$ is parametrized by the spherical coordinates $(\theta,\varphi) \in [0,\pi] \times [0,2\pi)$. For the previous three test cases, we use a cavity as illustrated in Fig. 3 as surface Γ. It is an open box of length $1 \times 0.25 \times 0.25\ m^3$ centered at the origin and open towards the positive x-axis.

In the convergence plots we use the following relative L^∞-norm over $\Omega \times \mathcal{D}$:

$$\frac{\|f - \mathcal{I}_M(f)\|_{L^\infty(\Omega\times\mathcal{D})}}{\|f\|_{L^\infty(\Omega\times\mathcal{D})}}.$$

Fig. 4 shows both the error behavior depending on M and the parameter range for three different values of k_{max} for the test case (i). Note that the number of basis functions needed to achieve some given tolerance increases linearly with k_{max}. As is expected the distribution of the parameter value resembles, at least visually, the usual interpolation point-sets and, up to a linear stretch, seems to be similar for all values of k_{max}.

In Fig. 5, we present the same plots as above but for test case (ii) and varying fixed wave numbers k. Again, observe the linear increase, with respect to k, of the recovered basis functions to achieve a certain tolerance and a similar parameter distribution for different wave numbers.

Figs. 6 and 7 illustrate the error behavior and the distribution of the picked parameters for cases (iii) and (iv). Similar observations as above can be made. Note that in the test case (iii) the parameter values are gathered around the value $\theta = \pi/2$ which corresponds to the equator of the sphere. Due to the spherical coordinates the parameter distribution is uniform on the sphere but not in the parameter domain. Concerning test case (iv), we observe that the most parameter values

Please cite this article in press as: M. Fares et al., The reduced basis method for the electric field integral equation, J. Comput. Phys. (2011), doi:10.1016/j.jcp.2011.03.023

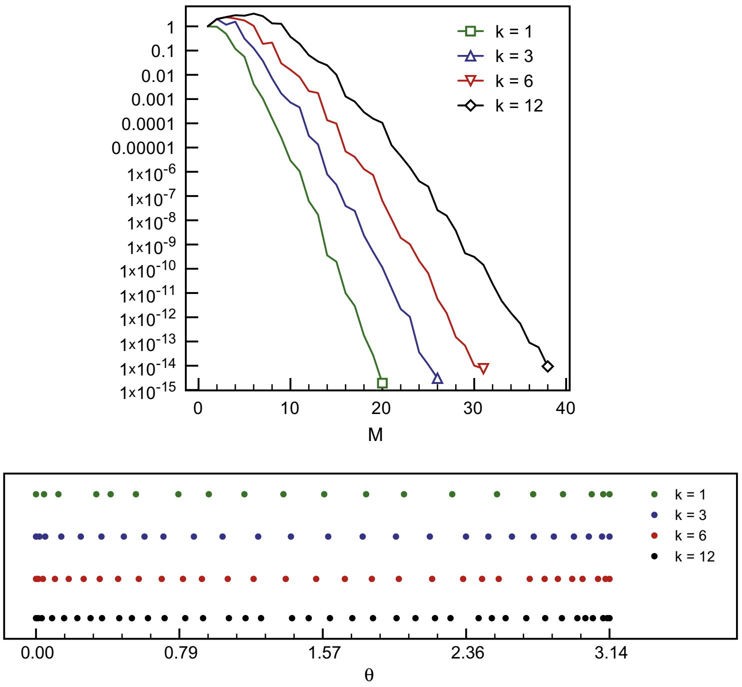

Fig. 5. Relative error in the test case (ii) for different values of k depending on the length M of the expansion (top) and the corresponding picked parameter values (bottom).

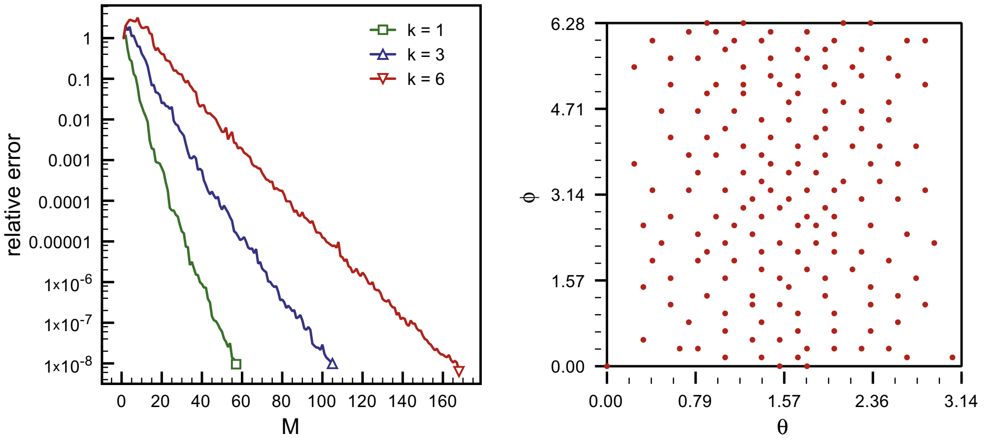

Fig. 6. Relative error in the test case (iii) for different values of k depending on the length M of the expansion (left) and the corresponding picked parameter values for $k = 6$ (right).

are picked around $k = 25$. This is due to the fact that the function under consideration is most oscillatory for the highest values of k. The greedy algorithm selects more points around high values of k in order to resolve the oscillations as expected.

5.2. Elementwise Empirical Interpolation Method (EEIM)

In the previous section, we observed that the dimension of the reduced basis space scales with the dimension of the parameter domain $\mathcal{D}$ and its volume. The expansion can become too large, i.e. large enough to significantly increase the computation time of the online procedure (Algorithm 2) which depends on M_k, M_f and M_R. This can increase the online computation time to be in the order of a direct boundary element computation. To overcome we propose an adaptive approach by splitting the parameter domain $\mathcal{D}$ into several subelements on which we approximate the subsequent function individually

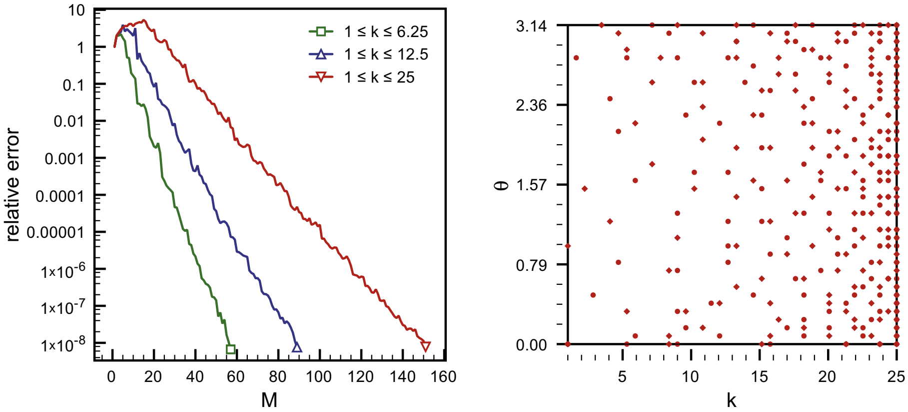

Fig. 7. Relative error in the test case (iv) for different values of k_{max} depending on the length M of the expansion (left) and the corresponding picked parameter values for $k = 25$ (right).

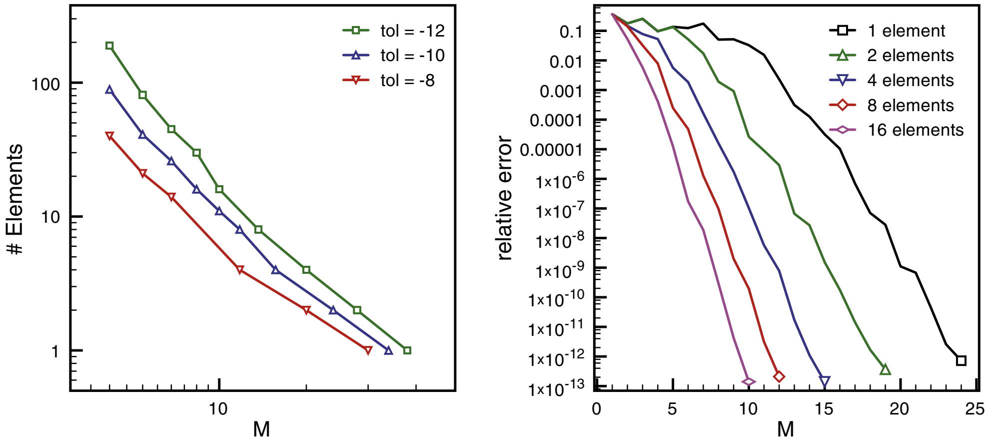

Fig. 8. The length of the EEIM expansion M versus the number of elements needed for test case (i) and three different error tolerances (left). Accuracy of the EEIM with respect of the length of the EEIM expansion M for different numbers of resulting elements (right).

by a different expansion of the form (13). It is similar in spirit to an *hp*-interpolant where *p* stands for the number of added modes per (parameter) subelement (indexed *M*) and *h* represents the diameter of the subelements. Observe that no inter-element continuity in the parameter domain is required.

The following approach is also discussed in further details in [12] where additionally a comparison to a similar approach, inspired by the techniques developed in [11], is given.

The overall strategy is the following. We first run the EIM to pick M parameter values $\mathbb{I}_M^1$, integration points $\mathbb{T}_M^1$ and basis functions $\mathbb{Q}_M^1$ which uniquely defines the interpolant on $\mathcal{D}$ using M terms. Next, if the interpolation error does not satisfy a certain given error tolerance we compute the gravity center of the point-set $\mathbb{I}_M^1$. The domain $\mathcal{D} \subset \mathbb{R}^d$ is then split into 2^d rectangular quadrilateral subelements $\mathcal{D}_i$ having the gravity center as common node. Otherwise if the tolerance is achieved, the previous computed expansion is final and remains unchanged. Finally, we proceed recursively on the newly created subelements. On each of them M new basis functions are computed following the greedy algorithm before we check the error tolerance etc. The algorithm is schematically described in Algorithm 5.

5.2.1. Numerical results

We present numerical test corresponding to the test cases (i) and (iv) of Section 5.1.1.

Fig. 8 illustrates the balance between the maximum length of the approximations M versus the number of elements needed to satisfy a certain given relative error tolerance for the test case (i). The error is measured in the relative L^∞-norm over the spatial domain Ω and the parameter domain $\mathcal{D}$. We also show the different accuracies with respect to the length of the interpolation series M for different resulting subdivisions of the parameter domain.

In a similar manner we plot the quantities in Fig. 9, but for test case (iv). Observe the algebraic relation between the required number of elements and the length of the expansion M.

Please cite this article in press as: M. Fares et al., The reduced basis method for the electric field integral equation, J. Comput. Phys. (2011), doi:10.1016/j.jcp.2011.03.023

Fig. 10 shows the picked parameter values and the corresponding subdivision for the test case (iv). The interpolant satisfies in all cases a relative error tolerance of 10^{-12}, but achieved with different maximum lengths of the expansions. The corresponding values of the lengths are $M = 218, 151, 106, 74$.

Algorithm:`EEIM`

```
Algorithm 5: The Elementwise Empirical Interpolation Method
Input: Function $f$, $\Omega$, $\mathcal{D}$, $M$, Tol.$*$/
/$*f : \Omega \times \mathcal{D} \rightarrow \mathbb{C}$: function to be interpolated$*$/
/$*M$: Maximal length of expansion per element$*$/
/$*$Tol: Tolerance$*$/
Output: A partition of $\mathcal{D} = \cup_{i=1}^{\mathcal{N}_E} \mathcal{D}_i$, $\mathcal{N}_E$ parameter samples $\mathbb{S}_M^i = \{\underline{\boldsymbol{\mu}}_{j,i}\}_{j=1}^M$ and interpolation points $\mathbb{T}_M^i = \{\underline{\mathbf{x}}_{j,i}\}_{j=1}^M$
begin
  $c = 1, \mathcal{N}^1 = 0, \mathcal{D}_1^1 = \mathcal{D}, \mathrm{Comp}_1^1 = 1, l = 1$
  while $c > \mathcal{N}^1$ do
    c = 0
    for $i = 1, \ldots, \mathcal{N}^1$ do
      if Comp$_i^l$ then
        /$*$Compute the interpolation error on element $\mathcal{D}_i^l$ $*$/
        $(\mathbb{I}_i^l, \mathbb{T}_i^l, \mathbb{Q}_i^l, \mathrm{Err}) \leftarrow \mathtt{EIM}(f, \Omega, \mathcal{D}_i^l, M)$
        if Err > Tol then
          /$*$Refine element $\mathcal{D}_i^l$ into $2^d$ subelements $*$/
          $\left(\mathcal{D}_{c+1}^{l+1}, \ldots, \mathcal{D}_{c+2^d}^{l+1}\right) \leftarrow \mathtt{REFINE}(\mathcal{D}_i^l, \mathbb{I}_i^l)$
          $\mathrm{Comp}_{c+i}^{l+1} = 1, \qquad \forall 1 \leqslant i \leqslant 2^d$
          c: = c + $2^d$
        else
            $c = c + 1$
            $\mathrm{Comp}_c^{l+1} = 0$
            $\left(\mathcal{D}_c^{l+1}, \mathbb{I}_c^{l+1}, \mathbb{T}_c^{l+1}, \mathbb{Q}_c^{l+1}\right) = \left(\mathcal{D}_i^l, \mathbb{I}_i^l, \mathbb{T}_i^l, \mathbb{Q}_i^l\right)$
        end
      else
            $c = c + 1$
            $\mathrm{Comp}_c^{l+1} = 0$
            $\left(\mathcal{D}_c^{l+1}, \mathbb{I}_c^{l+1}, \mathbb{T}_c^{l+1}, \mathbb{Q}_c^{l+1}\right) = \left(\mathcal{D}_i^l, \mathbb{I}_i^l, \mathbb{T}_i^l, \mathbb{Q}_i^l\right)$
          end
        end
      $l$: = $l$ + 1
    end
end
```

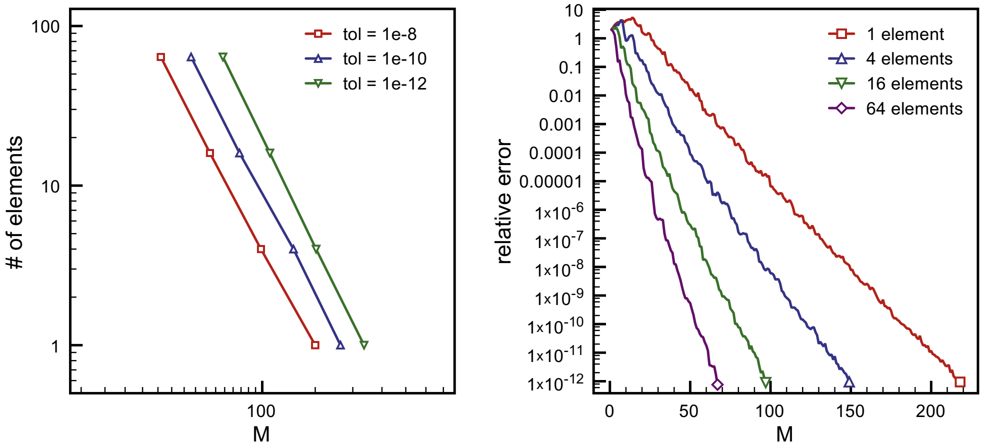

Fig. 9. The length of the EEIM expansion M versus the number of elements needed for test case (iv) and three different error tolerances (left). Accuracy of the EEIM with respect of the length of the EEIM expansion M for different numbers of resulting elements (right).

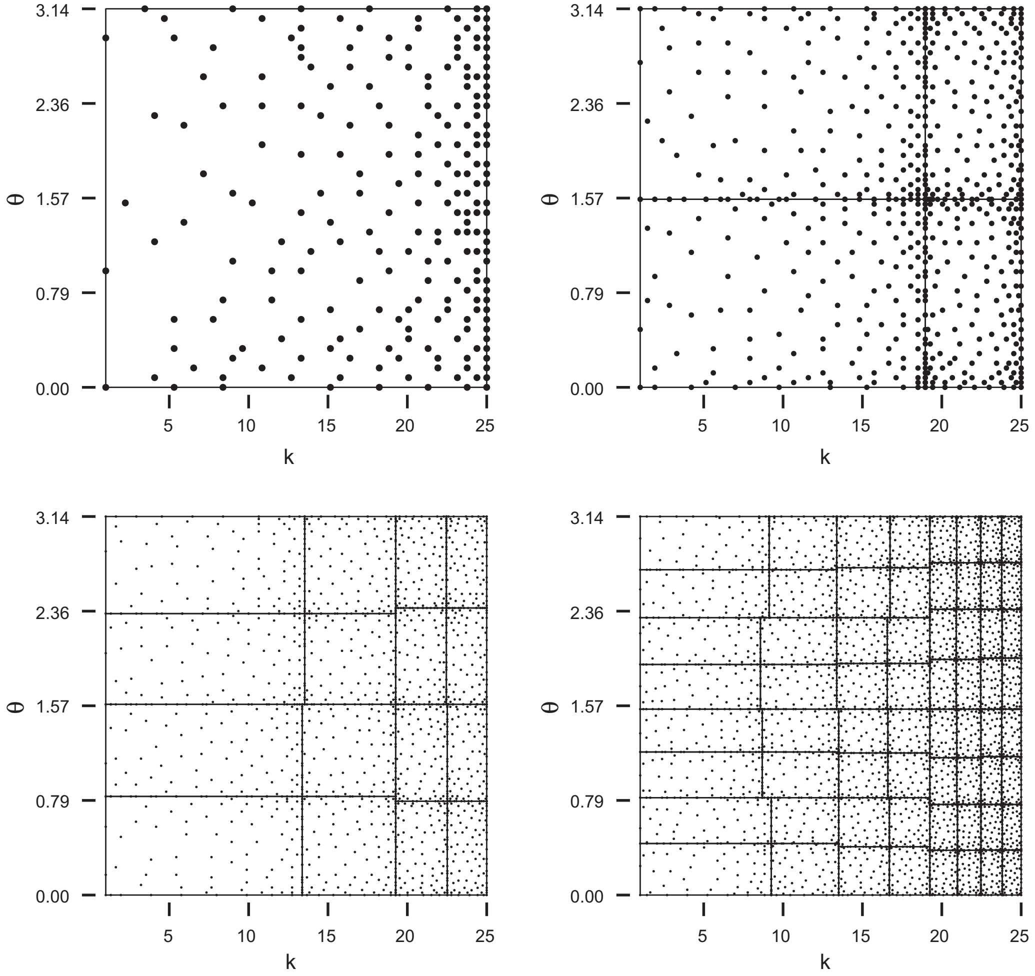

Fig. 10. Picked parameter values and subdivision of the parameter domain for different levels of refinements. The empirical interpolation satisfies a relative error tolerance of 10^{-12} for all four cases but with different lengths of the series per element, i.e. $M = 218, 151, 106, 74$.

6. Numerical tests of the reduced basis method

Finally, having all these tools to apply the reduced basis algorithm, we present some numerical examples.

```
Algorithm: Refine

  Algorithm 6: The Refine algorithm
  Input: $\mathcal{D}, \mathbb{I}$
  /* $\mathcal{D}$: parameter domain */
  /* $\mathbb{I}$: parameter samples in domain $\mathcal{D}$ */
  Output: A partition of $\mathcal{D}$ that consists of $2^d$ sub elements $(\mathcal{D}_1, \ldots, \mathcal{D}_{2^d})$
  begin
    Compute the gravity center $\tilde{\underline{\mathbf{x}}} = \frac{1}{\mathrm{card}(\mathbb{I})} \sum_{\underline{\mathbf{x}} \in \mathbb{I}} \underline{\mathbf{x}}$
    The subelements $\{\mathcal{D}_i\}_{i=1}^{2^d}$ is the unique partition of $\mathcal{D}$ consisting of rectangular quadrilaterals have as one common node $\tilde{\underline{\mathbf{x}}}$
  end
```

Please cite this article in press as: M. Fares et al., The reduced basis method for the electric field integral equation, J. Comput. Phys. (2011), doi:10.1016/j.jcp.2011.03.023

First, we consider the four following test cases:

Test case	Parameter	$\mathcal{D}$	Fixed values
(i)	θ	$\theta \in [0,\pi]$	$k = 5, 10, 20, \varphi = 0$
(ii)	θ, φ	$(\theta,\varphi) \in [0,\pi] \times [0,2\pi)$	$k = 5, 10, 20$
(iii)	k	$k \in [1,25]$	$\theta = \pi/4, \varphi = 0$
(iv)	k, θ	$(k,\theta) \in [1,25] \times [0,\pi]$	$\varphi = 0$

As scatterer, we use the geometry already introduced in Section 5.1.1 and illustrated in Fig. 3. The mesh used for the underlying truth approximation consists of 2236 elements/triangles with 3338 degrees of freedom (we shall present later an example with a more complex scatterer). The mesh-size is chosen in such a way that for the highest wavenumber considered, namely $k = 25\ \text{m}^{-1}$, we still have a sufficient resolution of the oscillations, i.e. 7 degrees of freedom per wavelength which yields an error of the truth solution (with respect to the exact solution) in the order of 10^{-1}. Note that this error is magnitudes larger than the errors arising form approximating the truth solutions by the reduced basis method in the framework of this study. The fact that the errors between the truth solution and the reduced basis approximation that go below 10^{-1} are of no practical interest, but remains interesting and important to analyze in a mathematical framework. The output functional is the RCS-signal given by the direction $\hat{\underline{\mathbf{d}}}$ parametrized in spherical coordinates by the angles $\theta_{\text{rcs}} \in [0,\pi]$ and $\varphi_{\text{rcs}} = 0$.

As underlying BEM-solver we use the code Cerfacs Electromagnetic Solver Code (CESC) developed at CERFACS, Toulouse. It solves the linear system using a LU-factorization, then solves for different right hand sides.

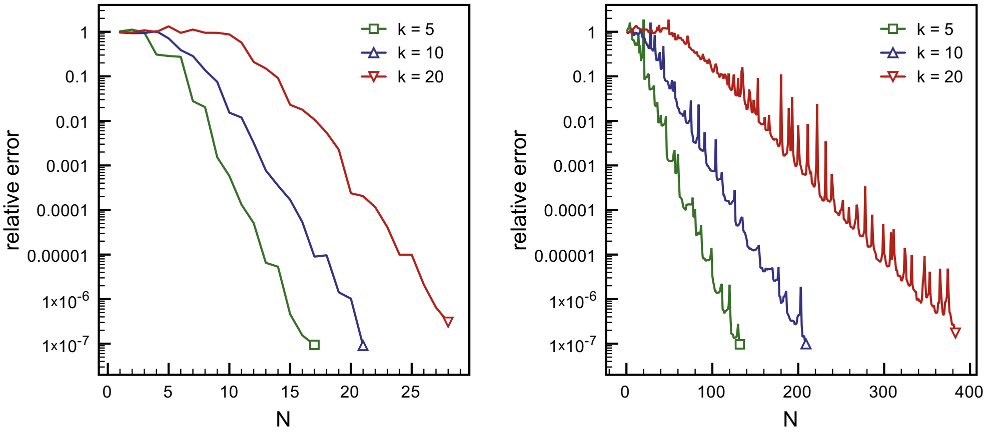

Fig. 11. Accuracy of the reduced basis method for test case (i) (left) and ii) (right) for different values of the wave number k.

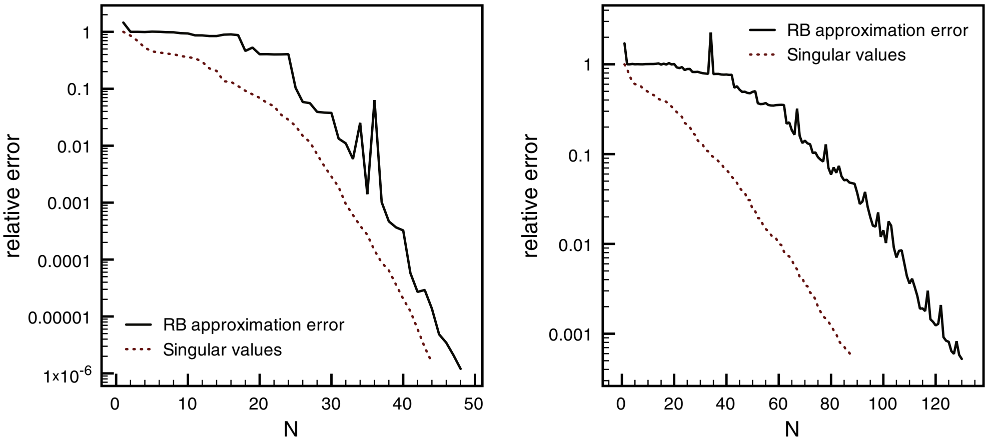

Fig. 12. Accuracy of the reduced basis method for test case (iii) (left) and (iv) (right) and comparison to the optimal accuracy given by the singular values.

Please cite this article in press as: M. Fares et al., The reduced basis method for the electric field integral equation, J. Comput. Phys. (2011), doi:10.1016/j.jcp.2011.03.023

In all the test cases, we study the relative error

$$\frac{\max_{\underline{\boldsymbol{\mu}}\in\Xi}\|\underline{\mathbf{J}}_h(\underline{\boldsymbol{\mu}})-\underline{\mathbf{J}}_N(\underline{\boldsymbol{\mu}})\|_{L^2(\Omega)}}{\max_{\underline{\boldsymbol{\mu}}\in\Xi}\|\underline{\mathbf{J}}_h(\underline{\boldsymbol{\mu}})\|_{L^2(\Omega)}}, \tag{14}$$

with respect of the increasing dimension N of the reduced basis space. Fig. 11 shows the error behavior for the test cases (i) and (ii) for three different values of the wavenumber k. In Fig. 12 the same quantity is illustrated for test cases (iii) and (iv). Observe the exponential convergence in all four cases. We also indicated the decrease of the singular values which represents the approximation properties of the best possible reduced basis in the sense of the $L^2(\Omega)\times L^\infty(\Xi)$-norm. Observe that the greedy-type of assembling the reduced basis is sub-optimal. However, it comes with a minimal assembling cost which is the true advantage of the greedy-algorithm. In addition, the error indicator has also an impact on the quality of the reduced basis. Therefore a more mathematical rigorous a posteriori estimate could also yield to a better performance of the reduced basis. However, this comment is of speculative nature.

Further we study CPU time of the online procedure and also compare it to solving the problems for each parameter value. We are focussing on test case (iv) where the RCS signal should be computed for all directions $\hat{\underline{\mathbf{d}}}$ parametrized in spherical coordinates by the angles $\theta\in[0,\pi]$ and $\varphi=0$.

We present the result of the reduced basis method with three different Empirical Interpolation Methods, i.e. we use three different types of EEIM interpolants. In the following table we present the number of EIM elements that are used for each interpolation for all three versions.

Version	Kernel function		Incident plane wave		RCS-signal	
	N. of elements	M	N. of elements	M_f	N. of elements	M_∞
1	1	148	1	15	4	98
2	4	98	4	9	16	66
3	16	67	8	8	64	47

In Fig. 13 we compare the average time of computing the RCS-signal using the different versions of the reduced basis method compared to the average computing time of the Boundary Element Method. For both methods the average computing time is taken over a sample set of parameter values. Regarding the Boundary Element Method we only compute the LU factorization once for all the parameter values having the same wavenumber, then we solve for the different right hand sides. We plot the speed-up of the reduced basis method in function of the dimension of the Reduced Basis. Observe that the speed-up can be considerably increased using an EEIM interpolant.

In the subplots of Fig. 14 we plot the absolute time for each parameter value (averaged over the whole set of parameter values) to compute the RCS signal in function of the dimension of the reduced basis. We subdivide the total computing time into the three most time consuming factors: The LU-factorization of the linear system (10), the computation of the residual error (12) and the computation of the RCS-signal. We not only observe that the total computing time is reduced while involving several EIM elements but also that the different fractions of computing times are slightly more equally distributed. However, the error tolerance of the EIM resp. EEIM is fixed in advance to 10^{-8}. Therefore one could further reduce the online

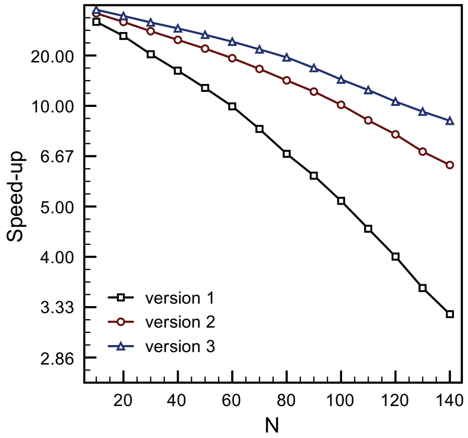

Fig. 13. Speed-up for three different versions of the online procedure of the reduced basis method with respect to the computing time using the Boundary Element Method in function of the dimension of the reduced basis. Test example (iv) is considered.

Please cite this article in press as: M. Fares et al., The reduced basis method for the electric field integral equation, J. Comput. Phys. (2011), doi:10.1016/j.jcp.2011.03.023

computing time by adapting the precision of the EIM resp. EEIM to the target error tolerance of the RBM. This would have the highest impact in the region with low values of *N* and thus lead to a higher speedup.

In Fig. 15 we plot the exact and approximated RCS-signal by the reduced basis method for test case (iii) with $k = 23.8$ and for three different dimensions of the reduced basis. We consider all directions $\hat{\underline{\mathbf{d}}}$ parametrized in spherical coordinates by the angles $\theta_{\mathtt{rcs}} \in [0, \pi]$ and $\phi_{\mathtt{rcs}} = 0$. In Fig. 16 we plot the RCS-signal corresponding to the first five reduced basis functions for the test case (iii).

Fig. 17 shows two different kinds of plots, (a) and (b), for the RCS-signal depending on the angle $\theta_{\mathtt{rcs}}$ of the direction $\hat{\underline{\mathbf{d}}}$ and the wave number *k*. We can observe that for some values of *k*, the RCS is changing fast in its neighbourhood. Fig. 18 provides a zoom of the region between $k = 12.5$ and $k = 13.5$ and we can detect a bifurcation of a branch.

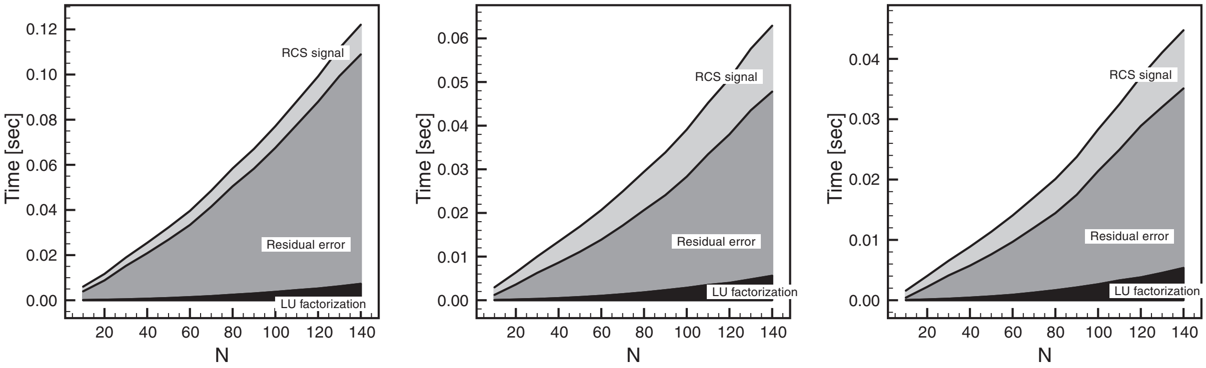

Fig. 14. The time of the subtasks of the online procedure of three different versions of the reduced basis method for different dimensions of the reduced basis. The time (measured in seconds) corresponds to the average computing time of the RCS-signal for a parameter value for the test example (iv).

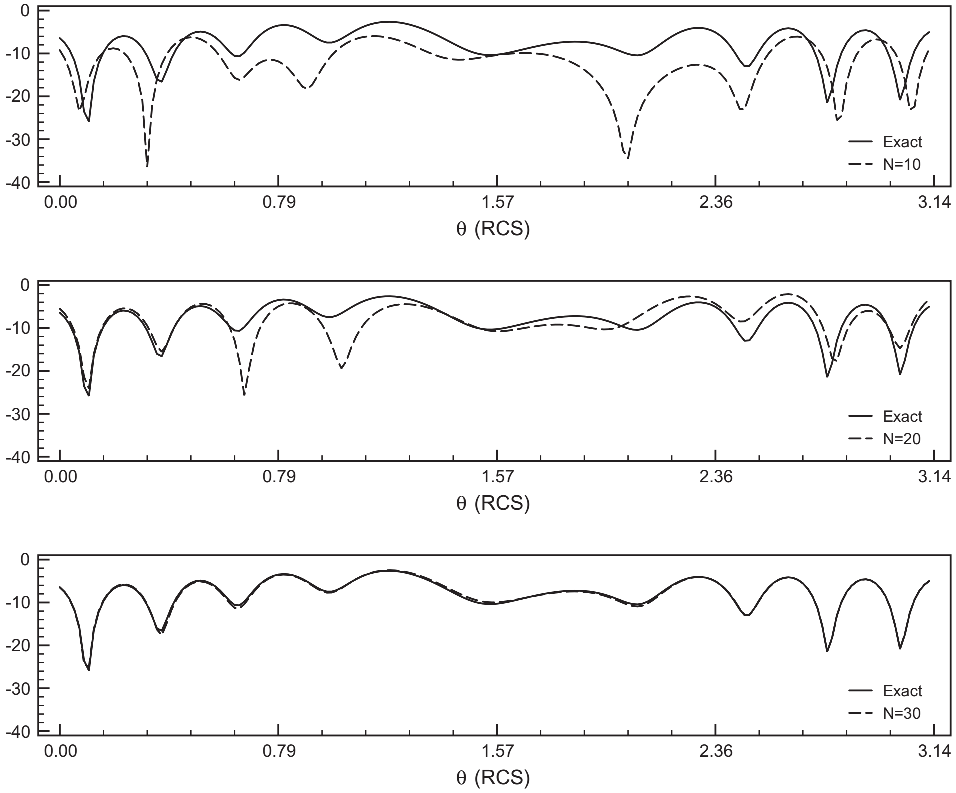

Fig. 15. Exact and approximated RCS-signal by the reduced basis method for test case (iii) with $k = 23.8$ and for three different dimensions of the reduced basis.

Please cite this article in press as: M. Fares et al., The reduced basis method for the electric field integral equation, J. Comput. Phys. (2011), doi:10.1016/j.jcp.2011.03.023

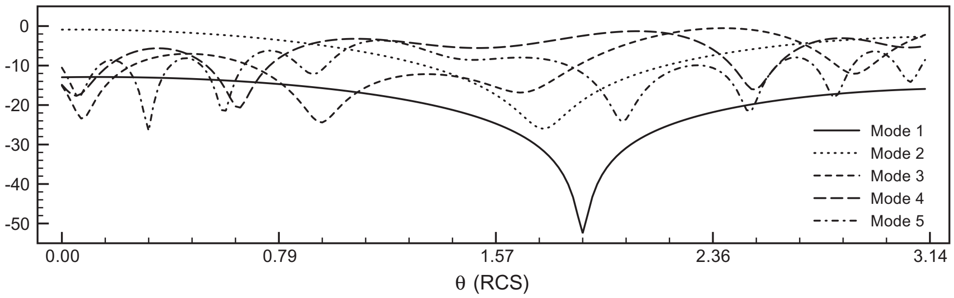

Fig. 16. RCS-signal corresponding to the first five reduced basis functions for test case (iii).

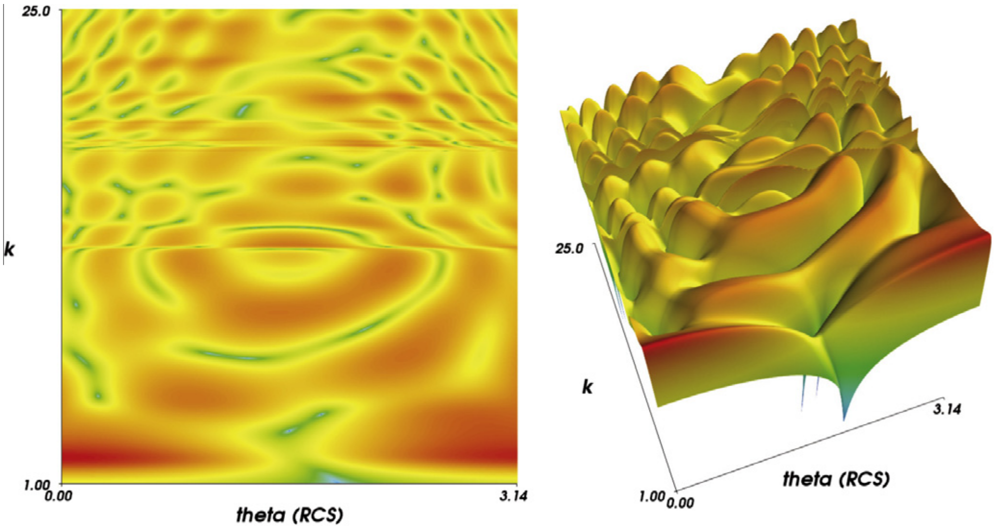

Fig. 17. Two different plots of the RCS-signal in function of the wave number $k \in [1,25]$ for test case (iii).

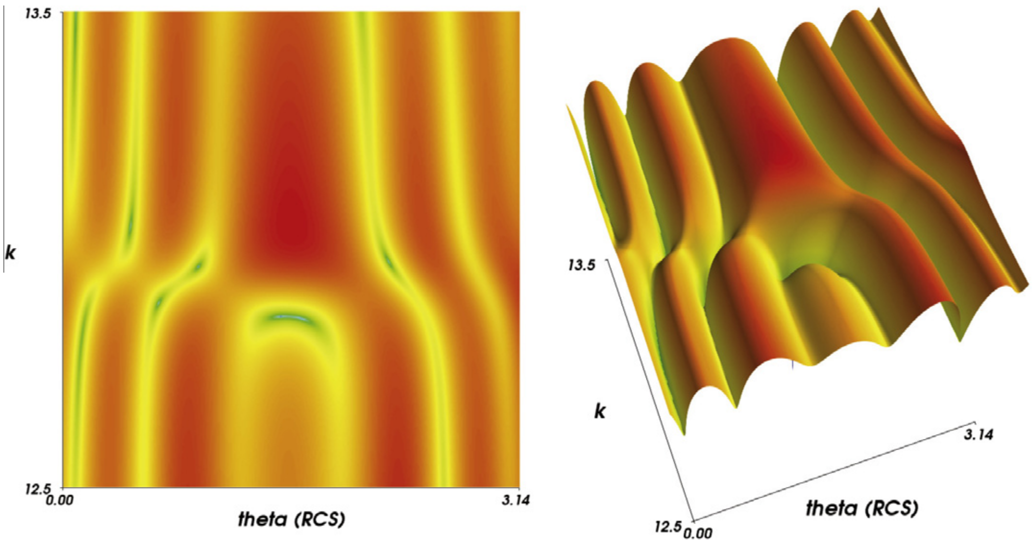

Fig. 18. Two different plots of a zoom of the RCS-signal in function of the wave number $k \in [12.5,13.5]$ for test case (iii).

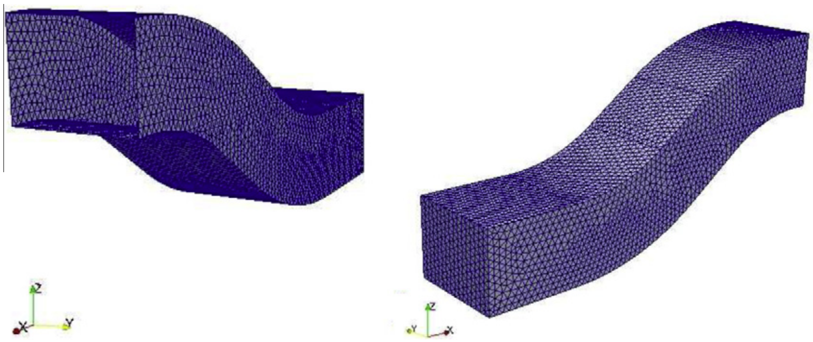

Fig. 19. Two different views of the scatterer used for the reduced basis test case (v).

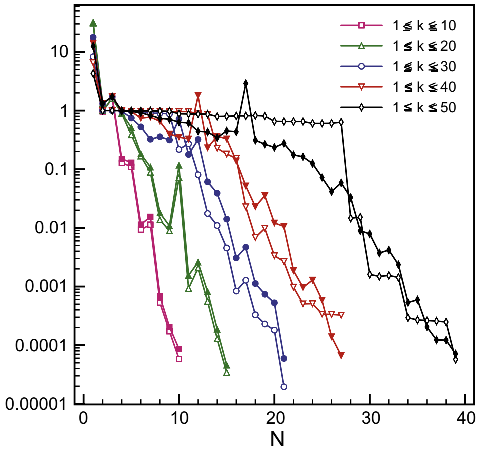

Fig. 20. Accuracy of the reduced basis method for test (v) and comparison between the error and the error indicator (filled symbols) for different parameter domains.

Finally, in test (v), we study a more complicated scatterer illustrated in Fig. 19 with a mesh consisting of 12′620 degrees of freedom. We analyze the case where the wave number is the sole active parameter:

Test case	Parameter	$\mathcal{D}$	Fixed values
(v)	k	$k \in [1, k_n]$	$\theta = \pi/4,\ \varphi = 0$

We construct the reduced bases for the five different parameter domains $[1, 10n]$ for $n = 1, \ldots, 5$. In Fig. 20 we illustrate the error between the truth solution and the reduced basis approximation (14) for all five different parameter domains and also compare it with the error indicator (12) (filled symbols). Observe that using the error indicator (12) seems to be justified, although not being optimal. Rigorous a posteriori estimates would further improve the estimation. It is hard to analyze the dependence of the dimension of the reduced basis N required for achieving a certain error tolerance with respect to k_n. The dimension depends in a sensible way on whether resonances occur or not. This depends on the geometry, the angle of the incident wave and of course the domain of wave numbers considered. There is no a priori theory which predicts the dimension of the reduced basis, it can only be empirically determined.

7. Conclusions

We presented an efficient algorithm to solve parametrized scattering problems in the form of the electric field integral equation (EFIE). The present algorithm consists of two steps: assembling the reduced basis, comparable to building a database, and a fast evaluation of the database in a many-query context. The advantage of such an approach is that, once the reduced basis resp. database is build, the evaluation of an output functional of the solution is independent of the dimension of the underlying discretization for any new parameter value. The parameters of the problem include the wave number, angle of the incident plane wave and its polarization.

Please cite this article in press as: M. Fares et al., The reduced basis method for the electric field integral equation, J. Comput. Phys. (2011), doi:10.1016/j.jcp.2011.03.023

For scatterers with volumes we are aware of the fact that spurious modes may interfere since we are using the EFIE. However, excluding them from the training sample Ξ avoids that the algorithm is at any point not well posed. We justify the use of the EFIE by the sake of its simplicity in the beginning of this project. However, there is no reason why the combination of the reduced basis method combined with any other standard solver for the parametrized scattering problem should not work. In particular, we will work on the Combined Field Integral Equation (CFIE) in near future.

The use of error indicators is important in the greedy algorithm to assemble the reduced basis. Therefore the quality of the estimate has a direct influence on the approximation properties of the reduced basis. It is ongoing work to develop mathematically rigorous efficient and reliable a posteriori estimates for the EFIE.

Acknowledgments

The authors thank Anne-Sophie Bonnet-BenDhia and Francis Collino for providing the Boundary Element Code CESC and for their collaborative effort.

The second author (Hesthaven) acknowledges partial support by OSD/AFOSR FA9550-09-1-0613, and by NSF, and DoE.

References

[1] B.O. Almroth, P. Stern, F.A. Brogan, Automatic choice of global shape functions in structural analysis, AIAA J. 16 (1978) 525–528.
[2] E. Balmes, Parametric families of reduced finite element models: theory and applications, Mech. Syst. Signal Process. 10 (4) (1996) 381–394.
[3] M. Barrault, Y. Maday, N.C. Nguyen, A.T. Patera, An ‘empirical interpolation’ method: application to efficient reduced-basis discretization of partial differential equations, C. R. Math. Acad. Sci. Paris 339 (9) (2004) 667–672.
[4] A. Barrett, G. Reddien, On the reduced basis method, Z. Angew. Math. Mech. 75 (7) (1995) 543–549.
[5] A. Buffa, S.H. Christiansen, The electric field integral equation on Lipschitz screens: definitions and numerical approximation, Numer. Math. 94 (2) (2003) 229–267 (for thin non-orientable “screens).
[6] A. Buffa, J. Ciarlet, On traces for functional spaces related to Maxwell’s equations. I. An integration by parts formula in Lipschitz polyhedra, Math. Methods Appl. Sci. 24 (1) (2001) 9–30.
[7] A. Buffa, J. Ciarlet, On traces for functional spaces related to Maxwell’s equations. II. Hodge decompositions on the boundary of Lipschitz polyhedra and applications, Math. Methods Appl. Sci. 24 (1) (2001) 31–48.
[8] A. Buffa, M. Costabel, D. Sheen, On traces for $H(\mathrm{curl},\Omega)$ in Lipschitz domains, J. Math. Anal. Appl. 276 (2) (2002) 845–867.
[9] Y. Chen, J.S. Hesthaven, Y. Maday, J. Rodríguez, Certified reduced basis methods and output bounds for the harmonic Maxwell’s equations, SIAM J. Sci. Comput. 32 (2) (2010) 970–996.
[10] S.H. Christiansen, Discrete Fredholm properties and convergence estimates for the electric field integral equation, Math. Comput. 73 (245) (2004) 143–167 (electronic, C-infinite surfaces).
[11] J.L. Eftang, A.T. Patera, E.M. Ronquist, An hp” certified reduced basis method for parametrized elliptic partial differential equations, SIAM J. Sci. Comput. 32 (6) (2010) 3170–3200.
[12] J.L. Eftang, B. Stamm, Parameter multi-domain “hp” empirical interpolation, NTNU Numerics, preprint 3/2011, Available from: <http://www.math.ntnu.no/preprint/numerics/2011/N3-2011.pdf>.
[13] A. Ern, J.-L. Guermond, Theory and Practice of Finite Elements, vol. 159, 2004.
[14] J.P. Fink, W.C. Rheinboldt, On the error behavior of the reduced basis technique for nonlinear finite element approximations, Z. Angew. Math. Mech. 63 (1) (1983) 21–28.
[15] L. Greengard, V. Rokhlin, A fast algorithm for particle simulations, J. Comput. Phys. 73 (2) (1987) 325–348.
[16] M.A. Grepl, Y. Maday, N.C. Nguyen, A.T. Patera, Efficient reduced-basis treatment of nonaffine and nonlinear partial differential equations, M2AN Math. Model. Numer. Anal. 41 (3) (2007) 575–605.
[17] M.D. Gunzburger, A guide to theory, practice, and algorithms, Finite Element Methods for Viscous Incompressible Flows, Computer Science and Scientific Computing, Academic Press Inc., Boston, MA, 1989.
[18] R. Harrington, Field Computation by Moment Methods, Macmillan Company, New York, 1968.
[19] R. Hiptmair, C. Schwab, Natural boundary element methods for the electric field integral equation on polyhedra, SIAM J. Numer. Anal. 40 (1) (2002) 66–86 (electronic).
[20] D.B.P. Huynh, G. Rozza, S. Sen, A.T. Patera, A successive constraint linear optimization method for lower bounds of parametric coercivity and inf–sup stability constants, C.R. Math. Acad. Sci. Paris 345 (8) (2007) 473–478.
[21] K. Ito, S.S. Ravindran, A reduced basis method for simulation and control of fluid flows, J. Comput. Phys. 143 (2) (1998) 403–425.
[22] L. Machiels, Y. Maday, I.B. Oliveira, A.T. Patera, D.V. Rovas, Output bounds for reduced-basis approximations of symmetric positive definite eigenvalue problems, C. R. Acad. Sci. Paris Sér. I Math. 331 (2) (2000) 153–158.
[23] Y. Maday, N.C. Nguyen, A.T. Patera, G.S.H. Pau, A general multipurpose interpolation procedure: the magic points, Commun. Pure Appl. Anal. 8 (1) (2009) 383–404.
[24] Y. Maday, A.T. Patera, D.V. Rovas, A blackbox reduced-basis output bound method for noncoercive linear problems, Nonlinear Partial Differential Equations and their Applications. Collège de France Seminar, vol. XIV (Paris, 1997/1998), Stud. Math. Appl., vol. 31, North-Holland, Amsterdam, 2002. pp. 533–569.
[25] Y. Maday, A.T. Patera, G. Turinici, A priori convergence theory for reduced-basis approximations of single-parameter elliptic partial differential equations, in: Proceedings of the Fifth International Conference on Spectral and High Order Methods (ICOSAHOM-01) (Uppsala), vol. 17, pp. 437–446, 2002.
[26] N.C. Nguyen, A.T. Patera, J. Peraire, A ‘best points’ interpolation method for efficient approximation of parametrized functions, Int. J. Numer. Methods Eng. 73 (4) (2008) 521–543.
[27] N.C. Nguyen, K. Veroy, A.T. Patera, Certified real-time solution of parametrized partial differential equations, in: S. Yip (Ed.), Handbook of Materials Modeling, Springer, 2005, pp. 1523–1558.
[28] A.K. Noor, J.M. Peters, Reduced basis technique for nonlinear analysis of structures, AIAA J. 45 (172) (1980) 487–496.
[29] J.S. Peterson, The reduced basis method for incompressible viscous flow calculations, SIAM J. Sci. Statist. Comput. 10 (4) (1989) 777–786.
[30] T.A. Porsching, Estimation of the error in the reduced basis method solution of nonlinear equations, Math. Comput. 45 (172) (1985) 487–496.
[31] C. Prud’homme, D. Rovas, K. Veroy, L. Machiels, Y. Maday, A. Patera, G. Turinici, Reliable real-time solution of parametrized partial differential equations: reduced-basis output bound methods, J. Fluid Eng. – T. ASME 124 (1) (2002) 70–80.
[32] S. Rao, D. Wilton, A. Glisson, Electromagnetic scattering by surfaces of arbitrary shape, IEEE Trans. Antennas Propag. 30 (3) (1982) 409–418.
[33] P.-A. Raviart, J.M. Thomas, A mixed finite element method for 2nd order elliptic problems, Applied Mathematical Sciences, Lecture Notes in Math., vol. 606, 1977, pp. 292–315.

Please cite this article in press as: M. Fares et al., The reduced basis method for the electric field integral equation, J. Comput. Phys. (2011), doi:10.1016/j.jcp.2011.03.023

[34] W.C. Rheinboldt, On the theory and error estimation of the reduced basis method for multi-parameter problems, Nonlinear Anal. 21 (11) (1993) 849–858.
[35] G. Rozza, Shape design by optimal flow control and reduced basis techniques: applications to bypass configurations in haemodynamics, Ph.D. Thesis, EPFL, 2005.
[36] G. Rozza, D.B.P. Huynh, A.T. Patera, Reduced basis approximation and a posteriori error estimation for affinely parametrized elliptic coercive partial differential equations: application to transport and continuum mechanics, Arch. Comput. Methods Eng. 15 (3) (2008) 229–275.
[37] K. Veroy, Reduced-basis methods applied to problems in elasticity: analysis and applications, Ph.D. Thesis, MIT, June 2003.
[38] K. Veroy, C. Prud'homme, A.T. Patera, Reduced-basis approximation of the viscous burgers equation: rigorous a posteriori error bounds, C. R. Acad. Sci. Paris, Série I 337 (9) (2003) 619–624.
[39] K. Veroy, C. Prud'homme, D. Rovas, A.T. Patera, A posteriori error bounds for reduced-basis approximation of parametrized noncoercive and nonlinear elliptic partial differential equations. AIAA, 2003.

Please cite this article in press as: M. Fares et al., The reduced basis method for the electric field integral equation, J. Comput. Phys. (2011), doi:10.1016/j.jcp.2011.03.023